Materials Today Bio 13 (2022) 100218

Contents lists available at ScienceDirect

Materials Today Bio

journal homepage: www.journals.elsevier.com/materials-today-bio

Nanomaterial-based biosensor developing as a route toward in vitro diagnosis of early ovarian cancer

Yuqi Yang [a,b,1], Qiong Huang [a,b,1], Zuoxiu Xiao [c,d], Min Liu [a,b], Yan Zhu [a,b], Qiaohui Chen [c,d], Yumei Li [e], Kelong Ai [c,d,*]

[a] Department of Pharmacy, Xiangya Hospital, Central South University, Changsha, Hunan, 410008, PR China
[b] National Clinical Research Center for Geriatric Disorders, Xiangya Hospital, Central South University, Changsha, Hunan, 410008, PR China
[c] Xiangya School of Pharmaceutical Sciences, Central South University, Changsha, Hunan, 410078, PR China
[d] Hunan Provincial Key Laboratory of Cardiovascular Research, Xiangya School of Pharmaceutical Sciences, Central South University, Changsha, Hunan, 410078, PR China
[e] Department of Assisted Reproduction, Xiangya Hospital, Central South University, Changsha, Hunan, 410008, PR China

ARTICLE INFO

Keywords:
Ovarian cancer
Early diagnosis
Biomarker
Immunosensor
In vitro diagnosis
Nanomaterials

ABSTRACT

The grand challenges of ovarian cancer early diagnosis have led to an alarmingly high mortality rate from ovarian cancer (OC) in the past half century. In vitro diagnosis (IVD) has great potential in the early diagnosis of OC through non-invasive and dynamic analysis of biomarkers. However, common IVDs often fail to provide reliable test results due to lack of sensitivity, specificity, and convenience. In recent years, the discovery of new biomarkers and the progress of nanomaterials can solve the shortcomings of traditional IVD for early OC. These emerging biosensors based on nanomaterials offer great improvements in convenience, speed, selectivity, and sensitivity of IVD. In this review, we firstly systematically summarized the limits of commercial IVD biosensors of OC and the latest discovery of new biomarkers for OC. The representative optimization strategies for six potential ovarian cancer biomarkers are systematically discussed with emphasis on nanomaterial selection and the design of detection principles. Then, various strategies adopted by emerging biosensors based on nanomaterials are also introduced in detail, including optical, electrochemical, microfluidic, and surface plasmon sensors. Finally, current challenges of early OC IVD are proposed, and future research directions on this promising field are also discussed.

1. Introduction

Ovarian cancer (OC) is the fifth leading cause of cancer-related death in females worldwide, accounting for 5% of all cancer-related deaths among women [1]. In 2020, more than 314,000 women worldwide were diagnosed with OC, and nearly 207,000 women died of OC [2,3]. The mortality rate of ovarian cancer now is still as high as 65.9% based on these latest data [4], which is almost indistinguishable in the past half century (Fig. 1A). On the contrary, the mortality rate of prostate cancer has dropped drastically by 58% from its peak in the 1970s (from 32.3% to 13.7%) thanks to the highly sensitive early in vitro diagnosis (IVD) for the specific prostate cancer biomarker (like prostate specific antigen) [5]. The same is true for other cancers such as stomach cancer [6]. One of the main reasons why the mortality rate of ovarian cancer is so different from other cancers is that ovarian cancer still lacks efficient early diagnosis methods. Currently, the diagnosis of OC mainly relies on imaging methods [7], which only detect mid-to-late OC because of the lack of high sensitivity and high resolution. Although the 5-year survival rate for early-stage ovarian cancer is as high as 90%, only 34% of early-stage ovarian cancers are successfully diagnosed (Fig. 1B and C). Therefore, there is an urgent need for an economical, efficient, and sensitive method for early diagnosis of ovarian cancer in clinical practice. IVD is attractive for early detection of OC because of their low cost and convenience. Nonetheless, many currently commercialized conventional marker-based IVD devices have high false positives and low efficiency in the early diagnosis of OC. More and more novel OC biomarkers with high specificity have been discovered with the in-depth study of the pathological process of ovarian cancer (Fig. 1D).

* Corresponding author. Xiangya School of Pharmaceutical Sciences, Central South University, Changsha, Hunan, 410078, PR China.
E-mail address: aikelong@csu.edu.cn (K. Ai).
[1] Yuqi Yang and Qiong Huang contributed equally to this work.

https://doi.org/10.1016/j.mtbio.2022.100218
Received 11 December 2021; Received in revised form 10 February 2022; Accepted 12 February 2022
Available online 15 February 2022

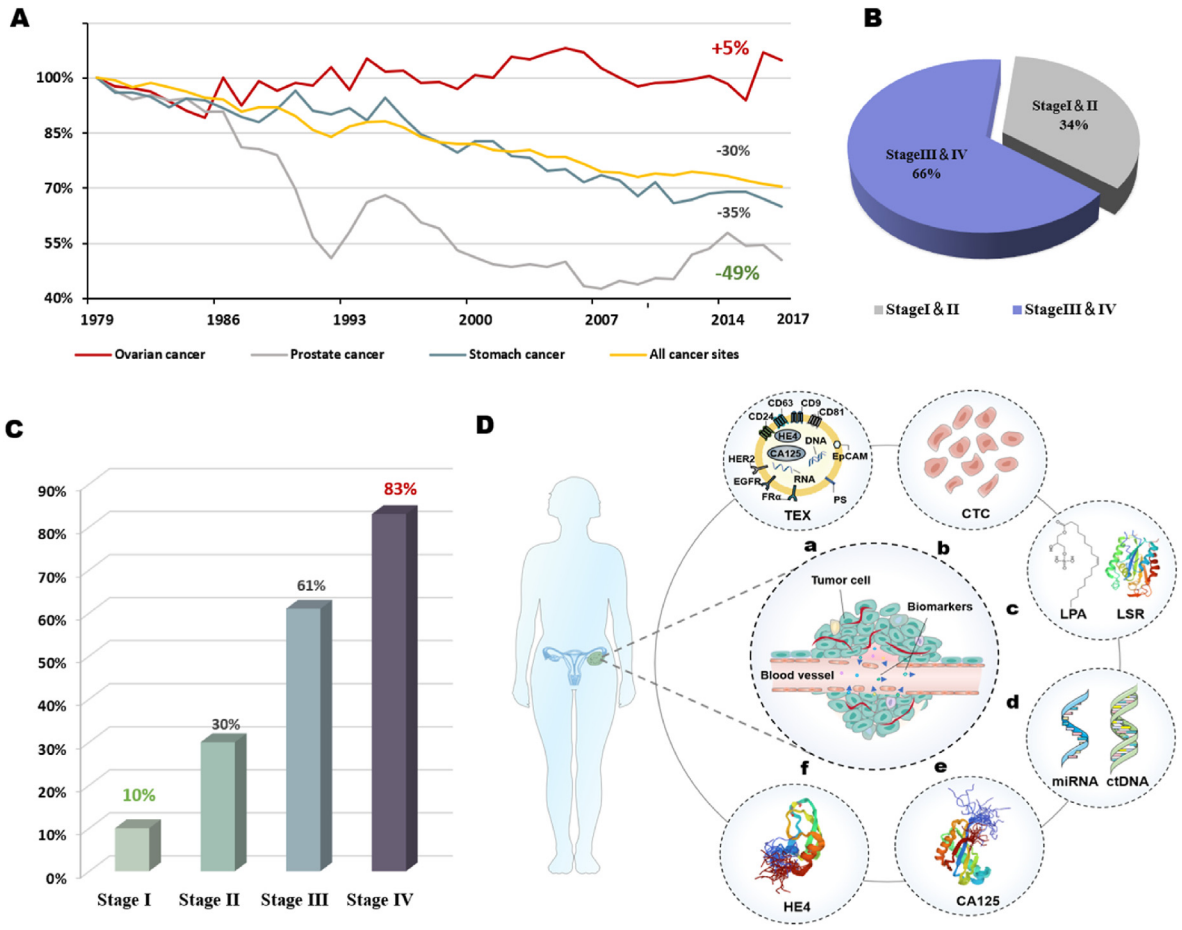

Fig. 1. (A) Changes in mortality of all sites, prostate, stomach and ovarian cancer. (B) Stage of ovarian cancer at diagnosis. (C) Mortality of different stages of ovarian cancer. (D) Biomarkers of research value in the blood of patients with ovarian cancer. Including emerging biomarkers: (a) TEX (b) CTC (c) LPA and LSR (d) miRNA and ctDNA, and classic markers: (e) CA125 (f) HE4.

The low abundance of these novel biomarkers among a high number of background hematologic cells represents the primary technical challenge for the realization of their detection and characterization. It has been a major focus of the field to develop methods with ultra-high sensitivity (refers to the responsiveness of a method to the substance to be tested, can be reflected by the lowest detection limit and the linear range), and specificity (refers to the selectivity and anti-interference ability of a method to the substance to be tested, can be reflected by the accuracy of detection). In recent years, the research of nanomaterials in the field of IVD technology has made great progress in improving the efficiency of early diagnosis of OC, while at the same time effectively overcoming the drawbacks in early diagnosis of OC [8,9]. Nanomaterials have a much larger specific surface area than bulk materials to be modified with different molecules. The rationale of using nanomaterials-based biosensor for OC biomarkers detection lies in the increased surface area available for contact between nanofeatures on the substrates and biomarkers, allowing for more binding sites to achieve highly efficient affinity capture. Moreover, nanomaterials have great flexibility in improving the detection sensitivity of these OC biomarkers because the properties of nanomaterials can be tuned by changing their size, shape, chemical composition, and surface functional groups. Remarkably, the IVD method allied multiple detection technologies can break through the bottleneck of traditional single technology by introducing a variety of nanomaterials, which now become a new trend in OC early diagnosis. Nevertheless, according to the characteristics of new OC biomarkers, how to construct an IVD device with high standards in economic, sensitive, fast, accurate, and other dimensions still faces great challenges.

Therefore, a systematic overview of the cutting-edge research in this field is critical. The main goal of this review is to highlight the current problems and challenges of the IVD for early OC and reveal that nanomaterials open up a new chapter in early diagnosis of OC. First, we introduce the current situation and bottleneck of IVD and comprehensively discuss the advantage of nanomaterials based IVD for OC early diagnosis. Subsequently, we highlight the progress in emerging nanomaterials-based IVD, which can be categorized according to seven types of potential biomarkers (Fig. 2). Lastly, we analyze the research gaps and put forward our perspective on the challenges and future research directions in these fields.

2. Advantage of nanomaterials-based IVD biosensor

IVD refers to the method of obtaining clinical diagnosis information by testing biological samples (especially blood) outside the human body. IVD has been widely used in cancer diagnosis and screening because of its convenience and cost-friendliness. Especially in developing countries, the application industry has made rapid progress [10]. The principle of IVD detection is that after the substance to be tested is added to the system, it will specifically bind to the biological recognition element, and the formed complex can cause the transducing element to generate various signals accordingly. Two key components for IVD are the identification and detection elements [11]. For recognition, the antibody–antigen interaction is usually used to capture protein biomarkers, or some small molecule probes are designed according to the specific structure of the biomarkers to bind the analyte by chemical force. For detection methods, transducer elements are used to convert the

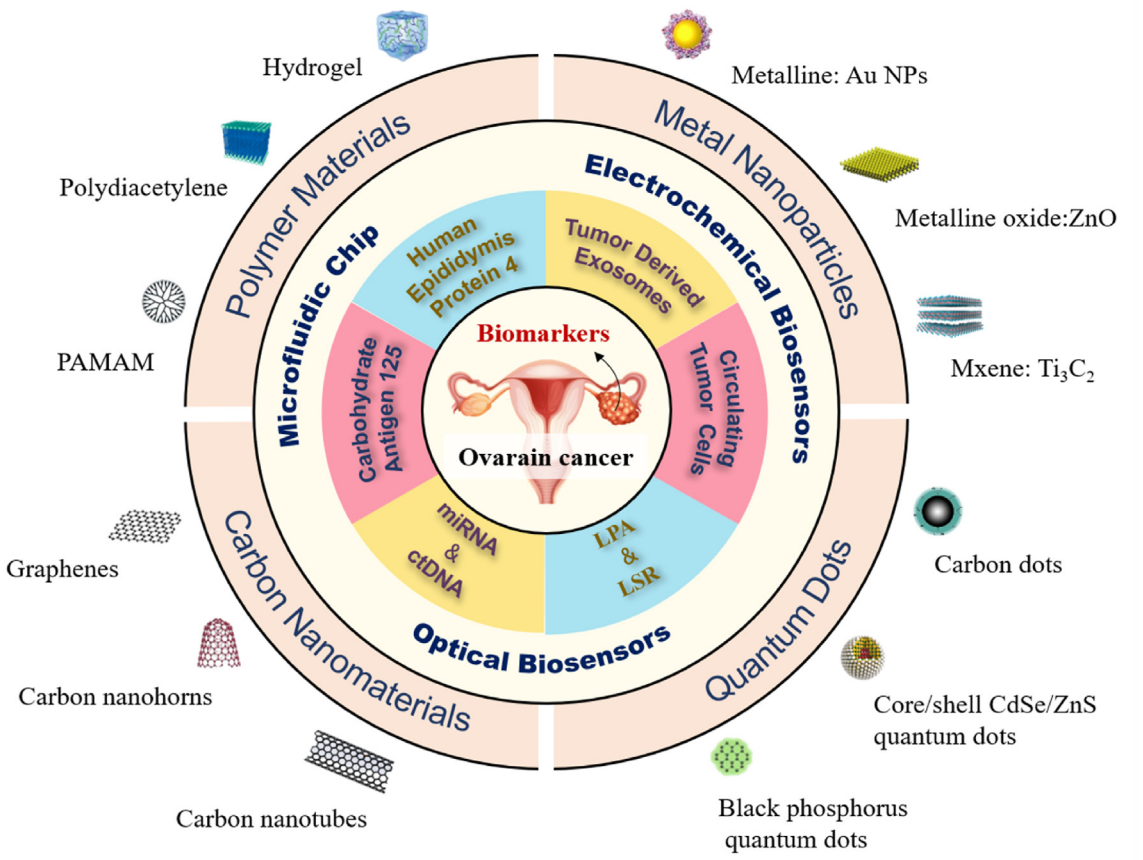

Fig. 2. The scope and focus of this article. OC is one of the most common cancers in women all over the world. The stage at the time of the diagnosis seriously affects the survival rate of ovarian cancer patients. IVD of biomarkers related to OC has become a breakthrough in the diagnosis of OC. Emerging biomarkers (TEX, CTC, LPA, LSR, metabolites, miRNA and ctDNA) and classic biomarkers (CA125 and HE4) show considerable potential. Various excellent detection technologies (such as microfluidic chip, optical biosensors and electrochemical biosensors) combined with nano materials (polymer materials, carbon nanomaterials, quantum dots (QDs) and metal nanoparticles) improve the detection performance of these biomarkers.

measured marker concentration level into a measurable output signal. Representative transducer elements include electrochemical sensors and optical sensors. The principle of electrochemical sensing is that the recognition element (such as antibody, aptamer) captures the target and forms an immune complex, which affects the electron transfer ability between the detection probe and the electrode, thereby generating or blocking current. The fixed electrode enriches and amplifies the electrochemical signal, establishes the linear relationship between the electrical signal and the concentration of the detected protein, and finally realizes the quantitative detection of the sample to be detected. Commonly used optical detection methods include colorimetric probes. The identification of the detection target is mainly based on the change of the ultraviolet–visible absorption spectrum after the interaction between the probe host and the object to be detected. When the absorption spectrum is in the visible light region, the color produced by the combination of the host and the guest Changes can be detected by the human eye. There are also detection probes developed based on the phenomenon of fluorescence resonance energy transfer (FRET). FRET is an analytical technique based on the phenomenon of energy transfer between two fluorescent molecules. When the emission spectrum of the donor fluorescent molecule overlaps with the absorption spectrum of the acceptor fluorescent molecule, and the distance between the two molecules is within 10 nm, a phenomenon occurs. FRET is a nonradiative energy transfer phenomenon, in which energy is transferred from the energy donor to the acceptor through dipole-dipole interactions, resulting in the fluorescence quenching of the donor's fluorescence. In addition, microfluidic chip is a new analysis method that integrates basic operation units such as sample preparation, reaction, separation, and detection in the medical analysis process into a micron-scale chip, and automatically completes the entire analysis process.

According to different transducers, the IVD biosensors of OC can be divided into optical sensors, electrochemical sensors, and surface plasmon sensors. Currently, some IVD biosensors have been commercialized and can be adopted in clinical laboratories for OC, like ADVIA Centaur (Siemens), Access 2 (Beckman Coulter), ARCHITECT i (Abbott Diagnostics), AxSYM (Abbott Diagnostics), VITROS (Ortho Clinical Diagnostics), AxSYM (Abbott Diagnostics), Elecsys (Roche Diagnostics) and VIDAS (BioMérieux) et al. [12]. Table 1 compares these devices in terms of the limit of detection (LOD), linear range, sample volume, and adopted technology (see Table 2).

However, currently IVD has not shown a survival benefit in the clinic because of the many biological and technical challenges associated with the detection of OC biomarker IVD in clinical samples. Firstly, the bottleneck in biology is that traditional OC biomarkers are not accurate enough for the diagnosis of OC, and false positives (because some biomarkers are also elevated in other diseases) and false negatives (because some biomarkers are also elevated in other diseases) are not accurate enough for the diagnosis of OC. In some cases, OC does not increase in the early stage). For example, HE4 is occasionally elevated in some gastric cancer and lung cancer patients, while CA125 is only elevated in 50% of early OC patients. Recently, some highly specific and sensitive OC biomarkers have been documented with further understanding of OC-related proteomics and genomics (e.g., tumor cell-derived exosome (TEX), CTCs, LPA, lipolysis-stimulated lipoprotein receptor (LSR), microRNAs (miRNAs), circulating tumor DNA (ctDNA), metabolites). IVD devices targeting these markers are still a new field to be developed.

Table 1
Commercialized diagnostic technology for OC.

Company	Instrument	Assay type	Marker	Normal Levels (U/mL)	LOD (U/mL)	Range (U/mL)
Siemens	ADVIA Centaur XP/CP	Paramagnetic particle-based chemiluminometric technology	CA125	<35	2	2~600
			CA15-3	<31	0.50	0.50~200
			AFP	<15	1.08	1.08~830
			CEA (ng/mL)	<5	0.5	0.5~100
			CA 19-9	<37	1.2	1.2~700
			βhCG	<0.005	0.002	0.002~1
			Estradiol (pg/mL)	<400[a]; <30[b]	11.8	11.8~3000
Beckman Coulter	Access 2	Chemiluminometric technology	CA125	<35	0.50	0.5 ~5000
			CA15-3	<31	0.50	0.5 ~1000
			AFP	<15	0.41	0.41~2478
			CEA (ng/mL)	<5	0.1	0.1~1000
			CA 19-9	<37	0.8	0.8~2000
			βhCG	<0.005	0.0005	0.0005~1
			Estradiol (pg/mL)	<400[a]; <30[b]	20	20~4800
Abbott	Architect i	Chemiluminescent microparticle immunoassay (CMIA)	CA125	<35	≤1.0	0~1000
			CA15-3	<31	0.5	0.5~800
			AFP	<15	0.33	0.33~290.5
			CEA (ng/mL)	<5	0.5	0.5~1500
			CA 19-9	<37	2	2~1200
			βhCG	<0.005	0.0012	0.0012~15
			HE4 (pmol/L)	<70[a] <150[b]	20	20.0~1500.0
			Estradiol (pg/mL)	<400[a]; <30[b]	≤10	0~1000
Ortho Clinical Diagnostics	Vitros	Immunometric immunoassay; chemiluminometric technology	CA125	<35	1.2	0~1000
			CA15-3	<31	0.5	0~500
			AFP	<15	0.5	0~500
			CEA (ng/mL)	<5	<0.45	0~400
			CA 19-9	<37	~	0~1000
			βhCG	<0.005	0.0005	0~1
			Estradiol (pg/mL)	<400[a]; <30[b]	6.36	6.360~3813.6
Abbott	AxSYM	Microparticle Enzyme Immunoassay (MEIA);	CA125	<35	2~600	
			CA15-3	<31	0.3	0.3~250
			AFP	<15	0.33	0.33~332
			CEA (ng/mL)	<5	0.5	0.5~500
			βhCG	<0.005	<0.002	~
Roche	Elecsys	Electrochemiluminescence immunoassay "ECLIA"	CA125	<35	0.6	0.6~5000
			CA15-3	<31	<1	1~300
			AFP	<15	0.5	0.5~1000
			CEA (ng/mL)	<5	0.2	0.2~1000
			CA 19-9	<37	<0.6	0.6~1000
			βhCG	<0.005	0.0001	0.0001~10
			HE4 (pmol/L)	<70[a] <150[b]	15	15~1500
			Estradiol (pg/mL)	<400[a]; <30[b]	5	5~4300
Biomerieux	Vidas	Enzyme-Linked Fluorescent Assay (ELFA)	CA125	<35	4	4~600
			CA15-3	<31	2	2~400
			AFP	<15	0.5	0.5~400
			CEA (ng/mL)	<5	0.5	0.5~200
			CA 19-9	<37	3	3~500
			βhCG	<0.005	0.002	0.002~1.5
			Estradiol (pg/mL)	<400[a]; <30[b]	9	9~3000

[a] Premenopausal.
[b] Postmenopausal.

Secondly, the technical bottleneck in the detection of OC biomarkers in clinical samples is low sensitivity. Primary ovarian cancer hangs deep in the abdominal cavity, and most of its specific markers have entered the ascites, except for some that can spread into the blood. Therefore, the concentration of specific ovarian cancer biomarkers in the blood is lower than other cancers. Detection of the biomarkers is more difficult in the early OC because cancer cells have not yet metastasized widely [13,14].

The unique properties of nanomaterials break through the "detection bottlenecks" stated above, and bring hope for optimizing IVD biosensors to achieve screening for early-stage OC. Firstly, nanomaterials can effectively improve detection sensitivity of biosensors for OC. Nanomaterials have a large specific surface area, to improve sensitivity by enriching the substances [15]. Moreover, some special nanoparticles have unique enzymatic activity to amplify the detection signal for biosensors [16,17]. For example, Fe_2O_3 nanoparticles have peroxidase-mimicking activity to amplify the electrical signal triggered by H_2O_2 [18], and graphitic carbon nitride nanosheets have the catalytic ability of luminol to amplify electrochemical signals [19]. Secondly, nanomaterials can increase the specificity of biosensors for OC by high flexible surface-modification functions. For example, graphene oxide (GO) is rich in active groups (e.g., carboxyl (-COOH), hydroxyl (-OH) and carbonyl (C═O)) [20], which can be modified and combined with

Table 2
Nanosensors for detecting biomarkers of ovarian cancer.

Category	Material	Method	LOD	Dynamic range
TEX	Microfluidic chip [37]	Microfluidics	/	/
	3D-nanopatterned microfluidic chip [38]	Microfluidics	<10 exosomes/μL	/
	ExoProfile chip [39]	Microfluidics	21 exosomes/μL	/
	PB-MXene [41]	Electrochemical	229 exosomes/μL	5.0 × 102 exosomes/μL ~ 5.0 × 105 exosomes/μL
	C-IONPs [42]	Electrochemical	125 exosomes/μL	6.25 × 102 exosomes/μL ~ 1.0 × 104 exosomes/μL
	Lum-AuNPs@g-C3N4 AuNFs [43]	ECL	39 exosomes/μL	1.0 × 102 exosomes/μL ~ 1.0 × 107 exosomes/μL
CTCs	Microfluidic chip [52]	Microfluidics	Capture efficiency: 90%	/
	Microfluidic chip [132]	Microfluidics	Capture efficiency: 98.1%	/
	PLGA -PDMS [53]	Microfluidics	Capture efficiency: A2780 91% OVCAR-3 89%	1~13 CTCs/mL
	Magnetic nanoprobes [62]	Immunomagnetic separation	Capture efficiency: 37.35% ~61.3%	/
	Magnetic nanoprobes [63]	Immunomagnetic separation	Capture efficiency: 92.5%	/
	PAMAM dendrimer SA-biotin [64]	Immunomagnetic separation	Capture efficiency: 90.3%	/
LPA	iPDAs [68]	Colorimetric	0.5 μmol/L	0.5 μmol/L ~ 8 μmol/L
	DCSH [67]	SPR + OWS	2 μmol/L	2 μmol/L ~ 30 μmol/L
LSR	CNHs/MMMJ/Cu NCs [72]	PEC	10-6 ng/mL	10 ng/mL ~ 10-6 ng/mL
	NiFe2O4NTs @BPQDs [71]	ECL	10-5 ng/mL	10-5 ng/mL ~ 100 ng/mL
miRNA	GO [91]	qRT-PCR	10 copies/mL	10~109copies/mL
	AuNPs [93]	Colorimetric	1 ng/μL	/
ctDNA	Microfluidic chip [92]	PCR	/	/
	DHN [94]	Electrochemical	KRAS:48.7 fmol/L BRAF: 44.1 fmol/L	KRAS:100 fmol/L~1 μmol/L; BRAF:100 fmol/L~0.1 μmol/L
CA125	Gold nanostructures [133]	Electrochemical	5.5U/mL	10 U/mL ~ 100U/mL
	AuNPs-reduced graphene oxide (RGO) [134]	Electrochemical	0.1U/mL	0.1 U/mL ~ 400U/mL
	Amidoxime-modified polyacrylonitrile nanofibers decorated with Ag nanoparticles [135]	Electrochemical	0.0042 U/mL	0.01U/mL ~ 350 U/mL
	MWCNTs-ZnO-NFs [106]	Electrochemical	0.00113 U/mL	0.001U/mL ~1 k U/mL
	Chitosan-AuNP/MWCNTs/GO [136]	Electrochemical	0.002 U/mL	0.01 U/mL ~ 100U/mL
	Silver-nanoparticles-graphene QDs [137]	Electrochemical	0.01U/mL	0.01 U/mL ~ 400U/mL
	3DN-CNT [109]	Fluorescence	0.01 U/mL	0.01U/mL ~ 1kU/mL
	CDs/AuNPs [113]	FRET	5.0 × 10−7 U/mL	1.0 × 10-6U/mL ~ 1.0 U/mL
	UCNPs/CDs [138]	FRET	9 × 10−3 U/mL	0.01 U/mL ~ 100 U/mL
CA125 +HE4 +IL6	Nanomagnetic beads [115]	GMR	CA125: 3.7 U/mL HE4: 7.4 pg/mL IL6: 7.4 pg/mL	CA125: 3.7 U/mL~ 100U/mL HE4: 7.4 pg/mL ~ 200 pg/mL IL6: 7.4 pg/mL ~ 200 pg/mL
CA125 +STIP1	RGO [139]	Fluorescence	CA125: 0.05 U/mL STIP1: 1 ng/mL	CA125: 0.1 U/mL ~ 2 U/mL STIP1: 1 ng/mL ~ 40 ng/mL
HE4	Graphene QDs [140]	FRET	4.8 pmol/L	4.8 pmol/L ~ 300 nmol/L
	Au NRs/NH2-GS Au@Pd urchin-shaped nanostructures [121]	Electrochemical	0.33 pmol/L	1 pmol/L~ 50 nmol/L
	CdSe/ZnS QDs [141]	Electrochemical	89 pmol/L	100 pmol/L ~ 2 nmol/L
	Magnetic microbeads [142]	Electrochemical	2.8 pmol/L	10 fmol/L ~ 100 μmol/L
	NiFe2O4 NTs [122]	ECL	3.3 fg/mL	10 fg/mL ~ 10 ng/mL
	TiO2MCs@RGO [123]	ECL	3.3 × 10−6 ng/mL	1.0 × 10−5 ng/mL ~ 1 μg/mL
	g-C3N4@ mesoporous SiO2 polymer dots@CNHs [143]	ECL	3.3 × 10-6 ng/mL	1.0 × 10-5 ng/mL ~ 10 ng/mL
	MoS2 NSs GCE/NiFe2O4NTs/AuNPs [124]	ECL + Colorimetric + Photothermal	3 × 10-7 ng/mL	10-6 ng/mL ~ 10 ng/mL
	AuNPs ZnCdHgSe QDs [144]	PEC	15.4 pg/mL	25 pg/mL ~ 4.0 ng/mL
	nPCN-224 MWCNTs/PDA/AuNP [126]	PEC	0.56 pg/mL	1.00 pg/mL ~ 10.0 ng/mL

various “capture molecules” (e.g., antibodies and aptamers) to recognize the biomarkers specifically. Moreover, the combined detection of multiple biomarkers can be achieved with nanomaterials-based biosensors by modifying different antibodies at nanomaterials [21], which greatly improve the specificity of the diagnosis of early OC. Thirdly, biosensors based on nanomaterials are more portable. Nanomaterials-based biosensors can not only be miniaturized, but can also achieve separation, capture and high-sensitivity detection in one thanks to the nano-scale and multi-functional characteristics of nano-materials, [22–24]. For example, the silicon microfluidic chip can be adopted as a complete analytical system for a rapid diagnosis by integrating the separation, delivery, and detection of several biomarkers of OC [25]. Many nanomaterials-based biosensors have been developed to IVD of early OC in recent years because of these unique advantages of nanomaterials. Currently, many kinds of biosensors are fabricated by various nanomaterials to detect several kinds of emerging biomarkers of OC such as TEX, CTC, LPA, LPS, nucleic acids (like, lncRNA, miRNA and ctDNA), metabolites (Fig. 3). In general, different markers have remarkably unique properties, and methods for their detection have been developed accordingly. Here, we systematically elaborate these nanomaterial-based ovarian cancer detection methods in the following 6 parts according to the types of ovarian cancer markers.

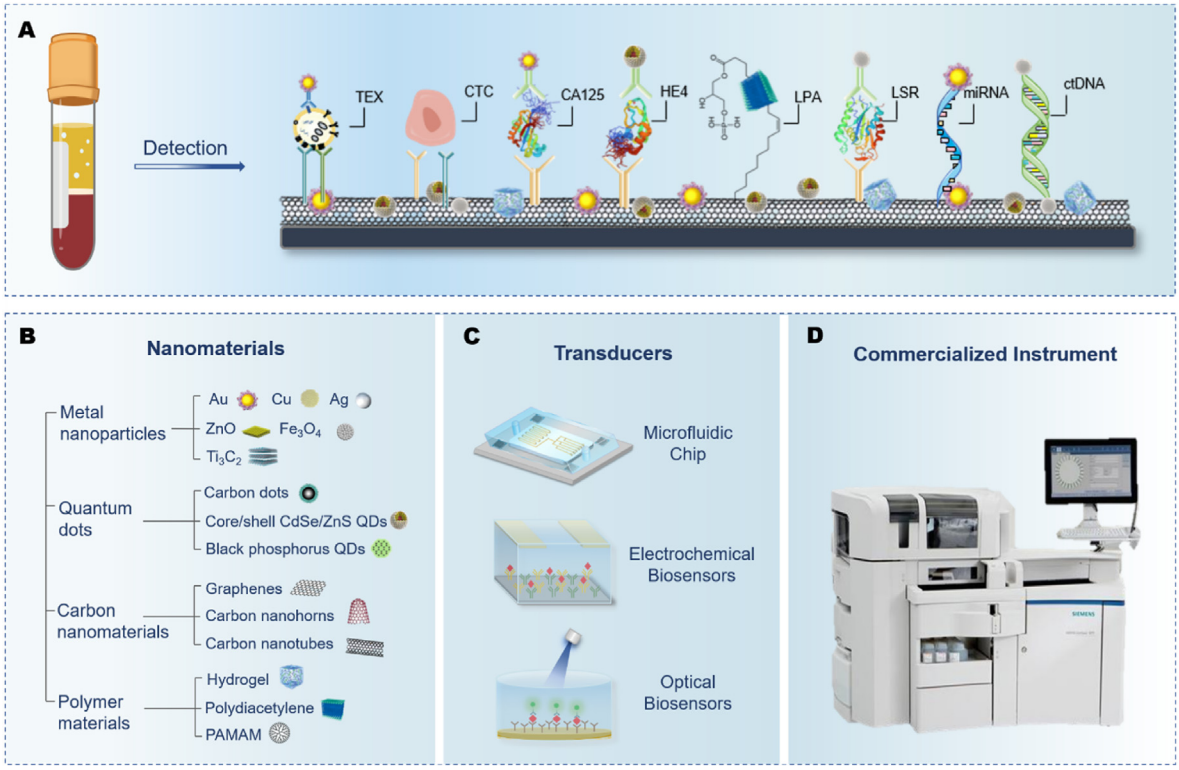

Fig. 3. Types of nanomaterials and sensors in the in vitro diagnosis of ovarian cancer. (A) The principle of capturing tested-biomarkers in the blood sample on the biosensors. (B) Types of nanomaterials in the in vitro diagnosis of ovarian cancer. (C) Types of sensors used in the in vitro diagnosis of ovarian cancer. (D) Large-scale commercialized IVD instrument.

3. Exosome

Exosome's secretion is greatly promoted by enhancing the docking between multivesicular body and plasma membrane in OC cells [26–28]. OC exosomes contain many kinds of membrane protein (like CD9, CD63, CD81, and CD82) [29–31] and various protein biomarkers which are highly expressed specifically in OC (CD24, CA125, EpCAM, and phosphatidylserine) [32,33]. At present, traditional methods such as high-speed centrifugal separation usually require complex sample preparation, dedicated analytical instruments, and large-volume samples [34,35]. However, the OC exosome content is very low in the blood, and the sensitivity of these methods is far below for early OC. In recent years, microfluidic chips and electrochemical immunosensors have attracted much attention for diagnosis of early OC with the advantages of convenient operation, simple instrumentation, and fast analyses. Ultracentrifugation and commercial exosome isolation kits usually cannot distinguish between exosomes derived from OC and exosomes derived from other cells (such as blood cells and other tissue cells). Microfluidics technology is a new type of automatically analytical method with integration the basic operation units of sample preparation, reaction, separation, and detection in the analysis process on a chip [36]. Recently, Kalpana et al. constructed a novel -channel-type microfluidic TEX-separation device modified with CD63 and EpCAM antibodies to effectively capture TEXs of OC [37]. The separation efficiency of TEX can further been improved by introducing nano-patterned channels (like herringbone nanochannel array [38] and 3D porous serpentine nanostructured microfluidic chip [39]) at microfluidic chips. For example, Zhang et al. developed a three-dimensional (3D) herringbone nanopattern (nano-HB) microfluidic chip for efficient separation and sensitive detection of TEXs [38] (Fig. 4A and B). The herringbone nanochannel array was prepared by the PDMS-based template method, and then the nanochannel was functionalized with anti-CD63, CD81 and EpCAM biotinylated antibodies. After the sample with 3, 3′-dioctadecyloxacarbocyanine perchlorate (DiO) dye-stained TEX was injected into the chip, the TEX surface protein marker was recognized specifically by the probe through antigen–antibody binding, and fluorescence was detected quantitatively. The herringbone nanochannel array greatly increased the probability of collision between the TEX surface and the probe. Simultaneously, the binding surface area and probe density were also increased greatly to improve the efficiency and speed of TEX binding (Fig. 4C–E). Therefore, the LOD of the nano-HB chip for TEX was extremely low (10 TEXs/mL) and 75% of TEXs could be captured in 100 μL of 10-fold diluted blood (Fig. 4F and G). In addition, the nano-HB chip combined with the sandwich exosome ELISA method successfully realized the integration of TEX separation and protein biomarker analysis on TEX, further optimized the detection process of TEXs. (Fig. 4H).

Electrochemical immunosensors are mainly composed of two parts: a fixed electrodes based on conductive nanomaterials modified with recognition element (e.g., antibody, aptamer) and an electrochemically active probe. Electrodes based on nanomaterials can greatly improve the sensitivity and selectivity of electrochemical immunosensors for TEXs due to the specific nanomaterials' advantages of high conductivity, high electrocatalytic activity, large specific surface area, and excellent stability [40]. For example, Zhang et al. developed a sandwich amperometric immunosensor based on a nanocomposite electrode composed of Prussian blue and Ti_3C_2 MXene (PB-MXene) for detection of OC exosome [41]. Multiple CD63 on the OC exosome membrane combined with rich CD63 aptamers on gold nanoparticles (AuNPs) and the PB-MXnene electrode to form an AuNPs-exosomes-PB-MXene-Apt sandwich structure, which generated a strong current signal by catalyzing the redox reaction of PB. Nevertheless, the LOD of the sandwich amperometric immunosensor was still only 229 exosomes/μL, which was much lower than that of microfluidic technology. Recently, Fatema et al. developed an ingenious electrochemical immunoprobe based on two different exosome biomarkers to further improve the detection sensitivity [42].

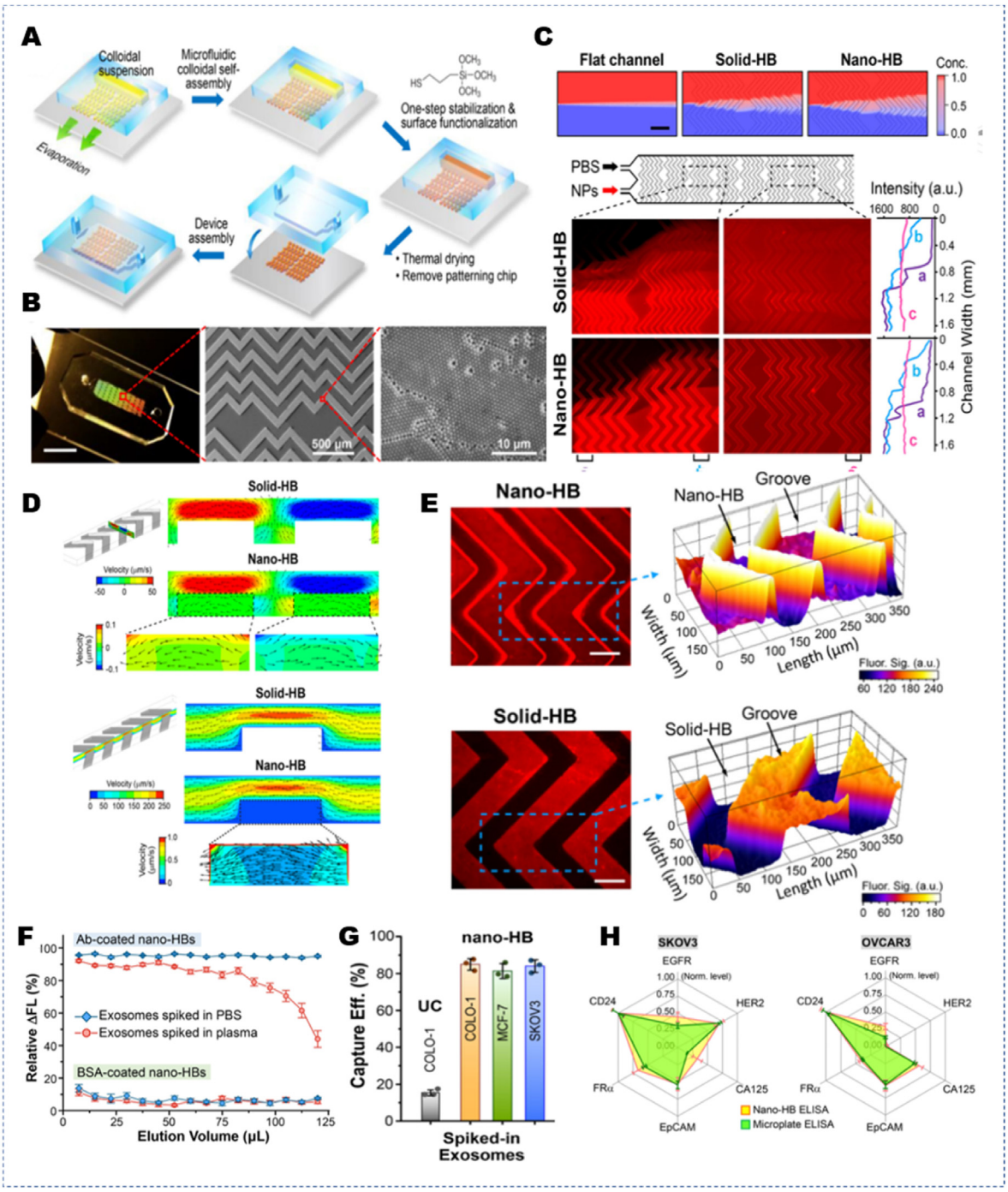

Fig. 4. (A) The workflow for fabricating a 3D nano-HB chip. (B) The SEM images of HB array patterned on a glass substrate with a crystalline nanoporous structure. (C) Simulation of mixing two streams of 50-nm nanoparticles (NPs) and water co-flowing in a flat-channel, solid-HB, or nano-HB device. (D) Simulation results show the transverse flow profiles across the channel width and the streamwise flow profiles along the channel length. (E) Representative 2D confocal microscopic images of the nano-HB (top) and solid-HB structures (bottom). (F) Representative 2D confocal microscopic images of the nano-HB (top) and solid-HB structures (bottom). (G) Comparison of standard UC isolation and the nano-HB capture of fluorescently stained exosomes of various cancer cell lines spiked in healthy plasma (10^6 μL^{-1}). (H) Comparing the nano-HB chip and a standard microplate kit for ELISA detection of six proteins in SKOV3 and OVCAR3 exosomes. Reprinted with permission from Ref. [38]. Copyright 2019, Springer Nature.

The CD9 aptamer and CA125 antibody were first modified on carboxyl group-functionalized iron oxide nanoparticles (C-IONPs) and screen-printed electrodes, respectively. The sandwich immune complexes generated highly sensitive current signals under the catalysis of the peroxidase-like properties from C-IONPs after addition of OC exosomes. The sensitivity of this method had been greatly improved, and its LOD was almost half that of the previous method (125 exosomes/μL), but it was still lower than the clinical requirement for early diagnosis of OC.

Electrochemiluminescence can greatly improve the sensitivity of electrochemical detection because of the unique advantages of optical signals. Liu et al. developed a sandwich-structure electrochemiluminescence (ECL) sensor to detect phosphatidylserine-positive exosomes for diagnosis of early OC [43]. The ECL sensor was composed of a glassy carbon electrode deposited with gold nanoflowers

(AuNFls) and the signal nanoprobe of graphitic carbon nitride nanosheets loaded with luminol-coated gold nanoparticles (Lum-AuNPs@g-C_3N_4). Abundant of the specific binding peptide (FNFRLKAGAKIRFRGC) of phosphatidylserine were first modified on AuNFls and Lum-AuNPs@g-C_3N_4 because of the high specific surface area of the AuNFls and g-C_3N_4. OC exosomes promoted the formation of a sandwich structure of AuNFls-exosomes-Lum-AuNPs@g-C_3N_4 to generate a strong chemiluminescent signal. Thanks to the advantages of ECL, the detection limit of the ECL sensor reached 39 TEXs/μL, which was close to the blood concentration of early ovarian cancer. Further, the ECL sensor had very excellent selectivity for OC with a significant different response to the exosomes of OC cells and HMRSV5 exosomes.

4. CTC

Recently, emerging evidence demonstrate that OC cells infiltrate the circulatory system like other types of cancer cells [44–46]. CTCs of OC can be detected in the peripheral blood of 93% of patients with early OC [47,48]. However, the number of CTCs is extremely low (only 1–10 CTCs/mL of blood in the early stage of OC, <100 CTCs/mL in the advanced stage of OC) in the blood [47]. CTCs also are easily destroyed during conventional separation and enrichment [49,50]. Recently, nanomaterial-based microfluidic technology and magnetic immune methods have shown very good separation efficiency and detection sensitivity [51]. For example, Chu et al. developed a 3D printed microfluidic device for enriching CTCs in OC blood samples based on the difference between blood cells (RBC and WBC) and CTC [52]. First, WBCs were effectively removed by modifying the CD45 antibody in the 3D channel of the microfluidic chip because all types of WBC high-expressed CD45 antigen. In addition, RBC were effectively removed by controlling the size of the microfluidic channel because the size of RBC was less than 3 μm. After these two steps, relatively pure CTCs (90%) were obtained. For improvement the separation efficiency of CTCs, Zeen et al. further fabricated a dual aptamer-modified poly (lactic-co-glycolic acid) (PLGA) nanofiber-based microfluidic device to separate and detect the mesenchymal OC cells A2780 and epithelial OVCAR-3 cells from OC blood samples [53]. The channel of the microfluidic chip was prepared by PLGA nanofibers modified with EpCAM-5-1 (high affinity for epithelial OVCAR-3 cells) and NC3S aptamers (high affinity for mesenchymal OC A2780 cells) through PDMS template method. The dual aptamer-modified microfluidic chip showed much better capture efficiency (91% for mesenchymal OC A2780 cells, 89% for OVCAR-3 cells), and sensitivity (92% for mesenchymal OC A2780 cells, OVCAR-3 cells 88%) than bare PLGA NFs based microfluidic chip. The microfluidic device even detected 1–13 CTCs/ml in clinical OC blood samples.

However, the complexity of the microfluidic chip preparation process limits its clinical application to a certain extent. Immunomagnetic nanoprobes had the advantages of low price and high efficiency for capture and detection of CTCs in the blood samples [54]. Currently, some commercial immunomagnetic nanoprobes have been developed for the detection of CTCs. For example, the anti-EpCAM antibody-modified magnetic beads based immunomagnetic CTC kit developed by CELLSEARCH (Huntingdon Valley, PA, USA) has been approved by the US Food and Drug Administration to separate CTCs from the whole blood of patients with cancer of the breast, colorectum, or prostate gland [55,56]. However, the CTC kit has low sensitivity for OC because of low EpCAM expression or EMT during metastasis in OC [57,58]. More than 95% of epithelial ovarian cancer (EOC, One of the most common OC subtypes) highly express folate receptor alpha (FRα) (high affinity for folic acid (FA)) [59,60]. Therefore, the immunomagnetic nanoprobes based on FA can capture CTCs from the blood more effectively than those based on EpCAM antibodies [61]. Recently, Fulai et al. developed a FA-modified bovine serum albumin (BAS)-decorated MNP probe to improve the CTC capture efficiency in the blood sample of OC [62]. Na et al. further improved the efficiency of capturing CTCs by combining two specific ligands (FA and EpCAM) to separate CTCs [63]. Recently, Meng et al. greatly increased the density of FA by grafting polyamidoamine (PAMAM) dendrimers-streptavidin (SA)-biotin-FA on the surface of magnetic nanoparticles to improve the efficiency of capturing CTCs [64]. Only a bit of FA-PAMAM usually were coated on MNPs because of the steric hindrance of MNPs when PAMAM dendrimers were conjugated directly to the surface of MNPs. To solve this problem, PMMA first modified the abundant FA and biotin through the amide bond, and then combined the modified SA-MMP to form PAMAM dendrimer-FA/biotin-SA-MMP. As a result, multiple FA molecules were connected to one MNP to greatly improve the capture efficiency of CTC because one SA molecule bonded to four biotin molecules with high affinity. Through this strategy, the capture efficiency of CTC had been greatly improved, up to 90.3% for OC.

5. LPA and LSR

LPA, as a biomarker of early-stage OC, has relatively high specificity and sensitivity. An increase of LPA concentration in the blood is observed in 90% of women with early OC and 100% of women with advanced OC [65]. However, the detection of LPA in the early OC serum is difficult because of low LPA concentration (<1.3 μM) [66]. Recently, Jie et al. developed a combination of surface plasmon resonance (SPR) and optical waveguide spectroscopy (OWS) to detect LPA with a dual-crosslinked supramolecular hydrogel (DCSH) [67]. DCSH coated on the gold surface had a tight structure because the polymer network contained β-cyclodextrin and ferrocene groups, where one ferrocene was embedded in two adjacent β-cyclodextrin cavities. The LPA, as a competitive guest, had a stronger binding affinity with β-CD than ferrocene, and destroyed the interaction between β-CD and FC to reduce the crosslink density of DCSH. Thus, the combination of LPA caused DCSH to swell to decrease the refractive index of DCSH. As a result, SPR-OWS detected LPA with the change of the plasmon resonance of the gold surface and the light reflectance. This method had high specificity and sensitivity for LPA detection (The LOD of this method was 2 μmol/L). Nevertheless, the detection limit of the method is still higher than the standard for early-stage ovarian cancer. In order to further improve the sensitivity, our research group designed a polydiacetylenes (PDA) sensor for highly sensitive detection of LPA according to all the properties of the LPA structure molecule [68]. The side chain of PDA bond to LPA with high specificity through electrostatic interaction and van der Waals force between the side chains of PDA and LPA, which led to the obvious color change of PDA. Thanks to this strategy, the sensitivity of the probe was greatly improved over the previous one, with a minimum detection limit of 0.5 μmol/L, which was already lower than the LPA cutoff value of 1.3 μmol/L for early OC.

Correspondingly, LSR, as the receptor of tumor lipid metabolism reprogramming, is also a specific early ovarian cancer marker. The membrane surface of OC cells is very rich in LSR [69,70]. The concentration of LSR in the blood also increases significantly with the infiltration of OC cells and the secretion of OC exosomes. Nevertheless, the LSR concentration is still low in the blood of early OC, about only higher than 9.0×10^{-5} ng/mL [71]. Therefore, it is difficult for many traditional detection methods to detect LSR in the OC blood samples [71]. For solve the problem, Fang et al. developed a photothermal enhanced ECL method based on black phosphorous quantum dots (BPQDs) and $NiFe_2O_4$ nanotubes ($NiFe_2O_4$NTs) to improve the sensitivity for LSR [71]. NiFe2O4NTs first were loaded with a large amount of BPQDs and N-(4-aminobutyl)-N-ethylisoluminol (ABEI) ($NiFe_2O_4$NTs@ABEI@BPQDs), and umbrella-shaped titanium dioxide/1-aminoethyl were loaded on the glassy carbon electrode (UST@ILs). The LSR antibodies were then modified on the $NiFe_2O_4$NTs@ABEI@BPQDs and UST@ILs. The addition of LSR promoted the formation of the special sandwich structure ($NiFe_2O_4$NTs@ABEI@BPQDs-LSR- UST@ILs) to trigger electrochemiluminescence. Furthermore, BPQDs mediated photothermal conversion to greatly enhance the ECL under 808 nm laser irradiation, and the temperature of the system also increased. Thanks to the strategy of

photothermal enhancement, the LOD was 1.0×10^{-5} ng/mL, which met the diagnosis requirements of early OC. Recently, Chen et al. further developed a multiple mixed TiO_2 mesocrystals junction (MMMJ) photoelectrochemical (PEC) colorimetric immunosensor for ultrasensitive detection of LSRs [72] (Fig. 5A). PEC had the advantages of low background, high sensitivity, and high signal-to-noise ratio for OC biomarkers. MMMJ was fabricated by depositing two different phases of TiO_2 mesogen layer-by-layer on carbon nanohorns (CNHs)-modified electrodes. Subsequently, copper nanoclusters (CuNCs) were introduced as sensitizers to further improve the PEC performance in the MMMJ. The strong interaction between different phase layers in MMMJ led to multiple amplifications of the signal to generate a more robust photocurrent response. The oxidation of benzoyl leuco methylene blue (leuco MB, as color-changing indicator) by H_2O_2 (from colorless to dark blue) was inhibited under light (Fig. 5B–D). [73]. In order to detect LSR, the LSR antibody was first modified on the surface of the PEC electrode. When LSR bond to the antibody of LSR, the catalysis of H_2O_2 was inhibited and the PEC current was reduced (Fig. 5E and F). Compared with previous methods, the sensitivity of this method was further increased (the LOD was 10^{-6} ng/mL).

6. Nucleic acids

OC continuously releases a lot of nucleic acids into the blood. Among them, circulating free DNA (ctDNA), miRNA with OC-specific sequences can be adopted as special biomarkers for early OC [74–77]. ctDNA has multiple types of DNA changes as the same as the gene mutation in the primary tumor lesion, including abnormal mutations, hypermethylation, microsatellite instability, and loss of heterozygosity [78]. The Cancer Genome Atlas reported that detection of mutant ctDNA had high sensitivity (>75%) and specificity (>80%) for the mutation of *TP53* in HGSOC patients [79]. Further, ctDNA can reflect the tumor conditions in the body specifically, accurately, and in real-time because the half-life of ctDNA is very short (16min-2.5h) [80–82]. miRNAs are small non-coding RNAs with a length of 20–25 nucleotides that are abnormally expressed in human OC [33,83,84]. Some of these miRNAs are down-regulated (e.g., miRNA-16 and miRNA-93), and some are up-regulated (e.g., miRNA-21, miRNA-221, miRNA-210, miRNA-200b, and miRNA-155) in OC patients [85–88]. However, the blood concentration of ctDNA or miRNA is ultra-low in early-stage OC (ctDNA is nM level, and miRNA <10 ng/μL). Traditional techniques have insufficient sensitivity and specificity for the detection of ctDNAs and miRNAs in the blood sample of early OC. Nanomaterials can improve the specificity and sensitivity of traditional methods by avoiding non-specific amplification, but also detect low-level nucleic-acid biomarkers directly in samples through light and electrical signals.

The traditional PCR method have the limitations of poor sensitivity and specificity for nucleic acids of early OC [89,90]. To solve this problem, Hu et al. fabricated a GO-based real-time fluorescent quantitative polymerase chain reaction (qRT-PCR) method for detecting miRNAs in OC [91]. GO had a high affinity with single-stranded DNA (ssDNA), and improved the sensitivity and specificity of qRT-PCR detection markedly by avoiding non-specific amplification. The LOD was 10-times lower than that of traditional qRT-PCR. Moreover, the accuracy of diagnosing OC was greatly improved, and the specificity was ≤100% when the method to jointly detect miRNA-210, miRNA-200b and miRNA-21. Recently, Guan et al. developed a microfluidic multiplex PCR sequencing technology for high-throughput and sensitive quantitative

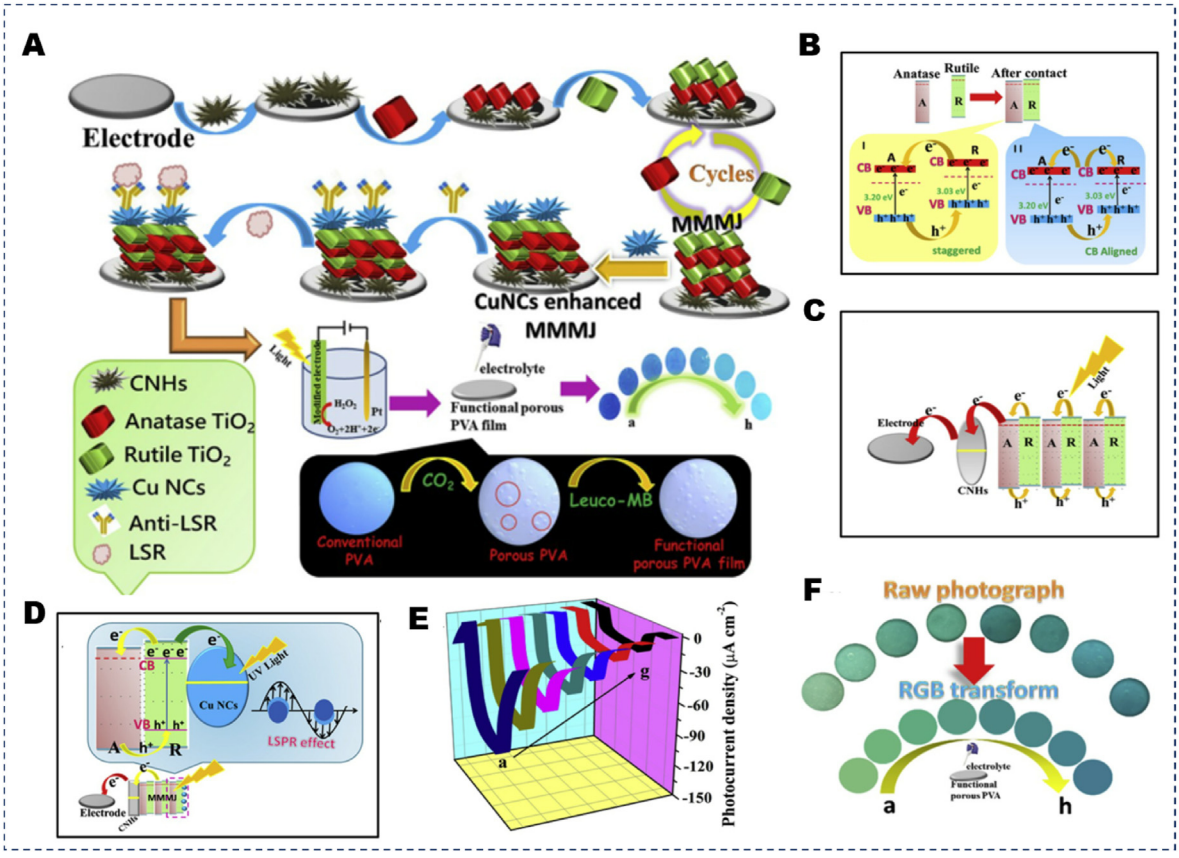

Fig. 5. Biosensor for LSR detection. (A) The illustration of the construction process of PEC biosensor. (B) Photocurrent generation mechanism in Anatase/Rutile TiO_2 mesocrystals junction. (C) The excited electrons transfer regulation in MMMJ. (D) Sensitive mechanism of CuNCs. (E) Photocurrent responses of the PEC biosensor toward different concentrations of LSR. (F) Color variations in leuco-MB functionalized colorimetric PVA films of the colorimetric biosensor. Reprinted with permission from Ref. [72]. Copyright 2019 Elsevier B.V.

detection of ctDNA for OC [92]. Different channels in microfluidic chips were designed to simultaneously detect sequence seven expected mutations in OC by PCR, which improved detection efficiency drastically. Input DNA as low as 0.2 fmol were amplified to produce ~10 fmol ctDNA through an integrated preamplifier. The overall sensitivity of the device to each mutation was 92% and the specificity was 100%.

The PCR method is relatively complicated and time-consuming for the detection of nucleic acid markers. Many colorimetric and electrochemical methods based on nanomaterials have been developed for nucleic acid detection for OC. For example, a fast colorimetric nanobiosensor based on gold nanoprobes was developed to detect miRNAs of OC [93]. miRNAs were combined with AuNPs-miRNA complementary probes to lead to aggregation of AuNPs and a red shift of AuNPs absorption spectrum. This method was adopted for highly sensitive detection of OC miRNA (miRNA and miRNA155) with a detection limit as low as 1 ng/μL. Recently, Chen et al. manufactured a DNA hexahedral-nanostructure (DHN) electrochemical biosensor for ctDNA detection in OC blood samples [94,95]. The DHN framework consisted of four single-stranded DNA probes (H1, H2, H3, H4), and each probe contained 30-mer polyA with a high affinity for gold electrodes. The ctDNA (*KRAS* and *BRAF)* [96]sequences hybridized with the unpaired ssDNA region on top of the DHN backbone and "fixed" the loose ssDNA to form a hexahedral structure. Simultaneously, the two auxiliary probes (A1 and A2) formed a complex with the G-quadruplex-hemin complex (GQHC)to catalyze the polymerization of electrochemically inactive aniline to conductive polyaniline (PANI). The formation of the G-tetramer-heme complex was hindered and the current response was strongly reduced if *KRAS* codon 12 or *BRAF* V600E mutation occur. The DHN electrochemical biosensor had high sensitivity and specificity for ctDNA of OC without complex amplification.

Long non-coding RNA HOX transcript antisense intergenic RNA (HOTAIR) is located on chromosome 12 within the homeobox C gene cluster. The interaction of HOTAIR and mitogen-activated protein kinase 1 regulates the proliferation, migration, and invasion of OC SKOV3 cells through miR-1, miR-214–3p and miR-330–5p. Detection of HOTAIR is critical for the early OC diagnosis in the body fluids of patients. However, there are currently two key analytical challenges: (1) low HOTAIR concentration levels (nM to fM range) and (2) analytical methods requiring a wide dynamic range (4–6 orders of magnitude). To this end, Narshone et al. developed a PCR-free assay based on simple colorimetric observation and electrochemical detection for the sensitive and specific detection of HOTAIR in OC [97] (Fig. 6A). First, streptavidin-coated magnetic beads selectively bond biotinylated functionalized HOTAIR complementary probes through biotin-avidin interactions to capture HOTAIR strands. The captured HOTAIR target was then magnetically purified and released from the capture probe by heating. The released HOTAIR sequences were double-stranded with HRP-functionalized self-assembled thiolated capture probes and captured onto the modified gold surface of screen-printed electrodes. HRP initiated the oxidation of TMB to form a blue charge-transfer complex, which not only allowed the presence of HOTAIR to be observed with the naked eye, but the color intensity was quantified by UV–vis at 652 nm. The blue product was further converted into a more stable electroactive yellow (diimine) complex to allow the amperometric quantification of HOTAIR using differential pulse voltammetry after addition of stop solution (acid). The assay showed excellent specificity (Fig. 6 B–C) and achieved a very low LOD of 1.0 fM HOTAIR with ranging from 10 fM to 1.0 nM in spiked buffer samples (Fig. 6 D-E). Notably, it was successfully applied to detect HOTAIR in

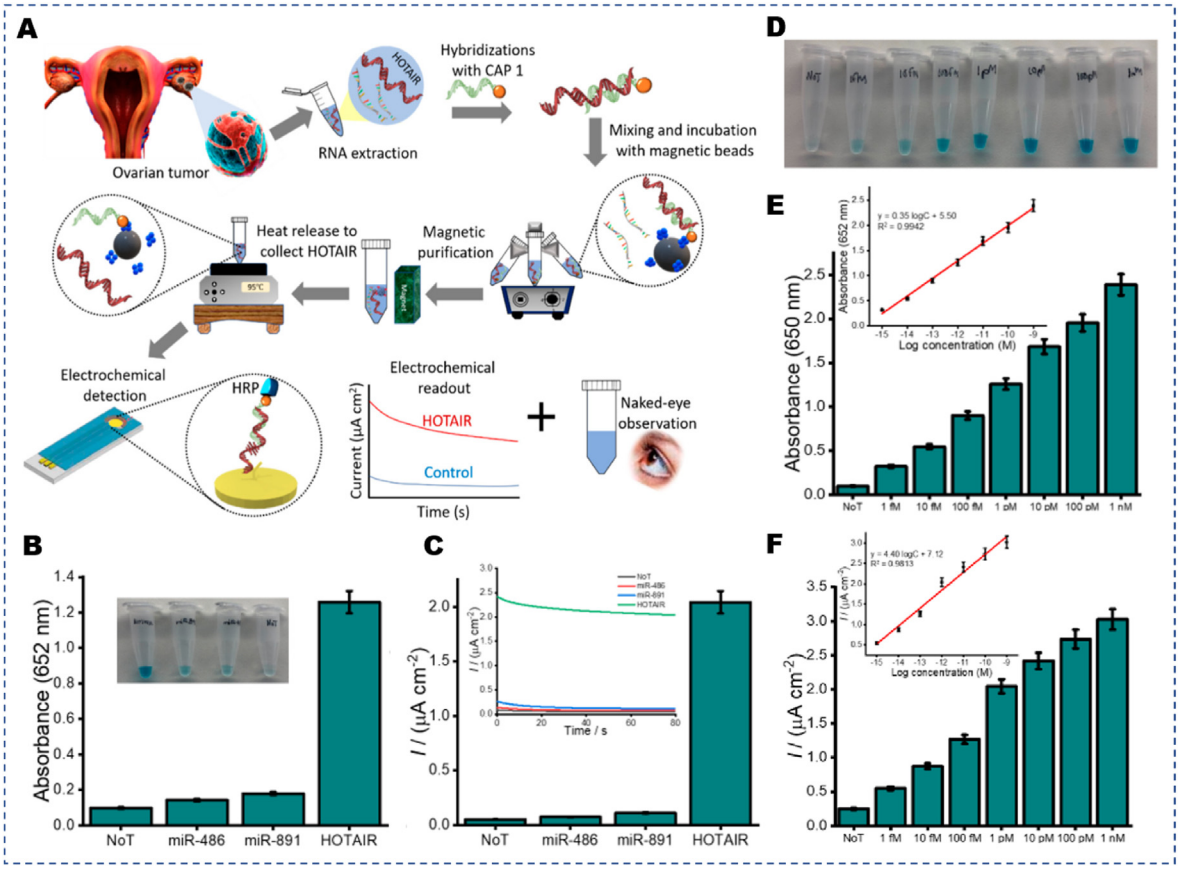

Fig. 6. Colorimetric observation and electrochemical detection of HOTAIR. (A) Schematic representation of the amplification free colorimetric detection of lncRNA. (B)–(C) Specificity of the assay. Bar diagrams indicate absorbance and current densities obtained in response to 1.0 pM of miR-486, miR-891, and HOTAIR sequences, respectively. (D)–(F) Sensitivity of the assay. They show visual inspection images, absorbance at 652 nm and amperometric current density of HOTAIR from a range of synthetic lncRNA sequences (1 fM), respectively. Reprinted with permission from Ref. [97]. Copyright 2020 by the authors.

cancer cell lines and a panel of plasma samples from ovarian cancer patients with satisfactory reproducibility.

7. Metabolites

Ovarian carcinogenesis alters metabolic pathways for biosynthetic and bioenergetic processes, resulting in dramatic metabolomic changes during OC progression. In particular, small molecule metabolites (molecular weight <1000 Da) as the final product of the pathway can accurately reflect the physiological state of the body. The levels of valine, phenylalanine, diethylketocarnitine, phenylalanine-phenylalanine dipeptide, polycarbonate and other small molecules in the blood of OC patients were significantly different from those of healthy individuals. Therefore, it is of great significance to construct a metabolic fingerprint based on biological fluids for the early diagnosis of OC.

Mass spectrometry (MS) has been widely used in metabolomics research due to the advantages of high accuracy, high sensitivity, high resolution, and high throughput. Laser desorption/ionization (LDI) mass spectrometry adopt the laser to irradiate a matrix to transfer the light energy to the samples, and then the sample molecules are desorbed and ionized and sent to the mass analyzer. Nano-scale plasmonic metal materials, metal oxides, precious metals and other emerging materials have been widely explored as LDI-MS substrates to detect small molecule metabolite fingerprints thanks to their excellent photoelectric energy conversion ability. For example, Su et al. used PdPtAu plasma alloy as a matrix to detect the metabolic fingerprint of gastric cancer [98]; Shu et al. developed a gold/dopamine plasma bubble chip for cervical cancer screening [99]; Huang et al. adopted Fe nanoparticles to diagnose lung adenocarcinoma [100]. Very recently, Pei et al. fabricated FeOOH@ZIF-8 nanocomposites as LDI-MS matrix by encapsulating FeOOH nanorods with zeolitic imidazolate framework (ZIF-8) crystals [101] (Fig. 7A). ZIF-8 modification reduced the rate of electron-hole recombination in FeOOH to significantly enhance the photocurrent response of the nanomaterials. FeOOH@ZIF-8 nanorods exhibited more efficient transfer of photon energy absorbed from UV laser to analyte than bare ZIF-8 or FeOOH. In addition, FeOOH@ZIF-8 nanorods exhibited a size-exclusion effect on large proteins to improve the specificity of detection of small metabolites. LDI-MS method with FeOOH@ZIF-8 as matrix demonstrated high intensity in detecting metabolites with selectivity and sensitivity for the analysis of small metabolites (alanine, valine, lysine, arginine, and sucrose) (Fig. 7B and C). The metabolic differences between OC patients and healthy controls were significant (AUC 0.9990, sensitivity was 97.24%, specificity was 98.67%) (Fig. 7D–F).

8. CA125

In addition to these novel OC biomarkers, some classic biomarkers can also be used to improve the sensitivity and selectivity of OC diagnosis through nanomaterials. CA125, also known as mucin 16 (MUC16), is a clinically widely used OC biomarker. Mechanical stretching of mesothelial cells leads to upregulation of CA125 expression in OC [102,103]. In health, CA125 cannot enter blood due to the connection between cells and the blocking effect of the basement membrane. The CA125 concentration in the serum of healthy people is very low (concentration <35 U/mL), but rises strikingly in early OC (~500 U/mL) and advanced OC (1000 U/mL) [104,105].

The detection sensitivity of electrochemical immunosensors of CA125 can be greatly improved by electroactive nanomaterials with a high specific surface, such as precious metal nanoparticles, polyaniline nanowires, carbon nanotubes, etc. For example, Brince et al. prepared multiwall carbon nanotube (MWCNT)-doped ZnO nanofibers (MZnONF) electrochemical sensors to detect CA125 with high sensitivity [106]. The MWCNTs-doped ZnO composite nanostructures MZnONF had higher conductivity and faster electron-transfer compared with individual MWCNTs or ZnO nanostructures [107,108]. The superior conductivity of MWCNTs enhanced the electron-transfer capacity between the detection probe and electrode, an improved the selectivity and sensitivity by increasing the amount of CA125 antibody immobilized on the electrode surface. The binding of CA-125 to the CA125 antibody at MZnONF electrode hindered the electron transfer of $[Fe(CN)_6]^{3-/4-}$ and weaken

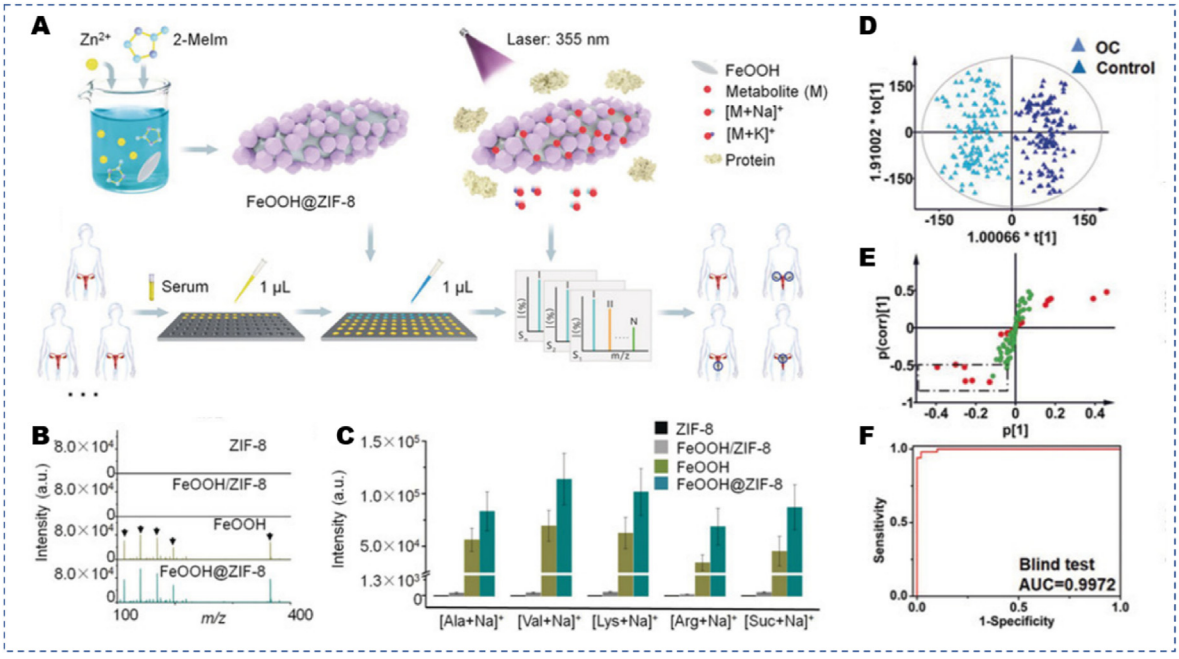

Fig. 7. (A)Schematic illustrations of synthetic route of FeOOH@ZIF-8 core-satellite nanocomposites and LDI-MS extraction of serum metabolic fingerprints. (B) Mass spectra of small metabolites mixture and (C) the mean intensities of their Na-adducted signals in 5 mg mL^{-1} BSA when using ZIF-8, FeOOH/ZIF-8, FeOOH, and FeOOH@ZIF-8 as matrix. (D) Orthogonal partial least-squares discrimination analysis score plots showing the global metabolic difference between 29 OC and 30 controls. (E) S-plots of OC vs. control. (F) Blind test based on the established models to differentiate 10 OC patients from 10 controls. Reprinted with permission from Ref. [101]. Copyright 2020 Wiley-VCH Verlag GmbH & Co. KGaA, Weinheim.

the DPV signal. The sensor had very high sensitivity and selectivity thanks to the excellent characteristics of MZnONF, and the LOD was far below the threshold required for early OC (0.00113 U/mL vs 500 U/mL). Nanomaterials can also greatly improve the sensitivity of fluorescence detection of CA-125. For example, Vinayakumar et al. developed a detection 3D carbon nanotubes (3DN-CNT) platform for CA125 based on ssDNA aptamer fluorescent probes [109]. The ssDNA aptamer (rCAA-8) linked to carboxy-fluorescein (FAM) was used as fluorescent dyes. The rCAA-8 specifically recognized the conservative region of CA125 without affecting the affinity of antibodies [110–112]. Importantly, 3DN-CNT facilitated the attachment of rich antibodies to capture CA125 due to the large surface area of 3DN-CNT, which caused a great fluorescence enhancement to sensitively detect CA125. In addition, Somayeh et al. developed a fluorescence resonance energy transfer (FRET) probe based on carbon quantum dots (CDs, as energy donors) and gold nanoparticles (AuNPs, as energy acceptors) for highly sensitive detection of CA125 [113]. CDs were first modified with CA125 aptamer, and then CA125 promoted FRET through the formation of a sandwich-type complex of AuNPs-PAMAM-CA125 antibody/CA125/CDs-aptamer. AuNPs "wrapped" with PAMAM dendrimers greatly increased the sensitivity of the FRET sensor by attaching rich CA125 antibody molecules.

However, CA 125 is not only elevated in OC blood, but also in other diseases and about 5% of healthy women [114]. Recently, Todd et al. developed a silica coated giant magnetoresistive (GMR) biosensing system for the combined detection of three OC biomarkers (CA125, HE4, and IL6) to improve the accuracy and reliability of OC early diagnosis [115]. CA125, HE4, and IL6 antibodies were first connected to the three GMR sequence sensors to capture the corresponding biomarkers. The three biomarkers cause the magnetic nanoparticles to be connected to the GMR sequence sensors by forming a sandwich complex, which changed the resistivity of the GMR for the detection of the three biomarkers (Fig. 8A). This method synchronously achieved multiplex detection of CA125, HE4, and IL6, with a LOD as low as 3.7 U/mL, 7.4 pg/mL, and 7.4 pg/mL, respectively (Fig. 8B). The positive predictive value of combined detection of CA125, HE4, and IL6 for OC diagnosis was 92.3%, which met the needs of accurate diagnosis of early OC. Moreover, the nanomaterial-based GMR sensor was easy to miniaturize and had great commercial prospects (Fig. 8F–I).

8.1. HE4

HE4, as a secreted glycoprotein encoded by WFDC2, is highly expressed in EOC cells, but not or low in other types of OC (for example, mucinous carcinoma, clear cell carcinoma, or benign ovarian disease) and normal tissues [116,117]. The normal range of the blood concentration of HE4 in premenopausal women is <70 pmol/L, whereas the blood concentration is ~100 pmol/L in early OC and reaching 500 pmol/L in advanced OC [118,119]. Currently, the HE4 has been approved by the Food and Drug Administration for monitoring OC patients [120]. Different nanomaterials have been widely adopted in the electrochemical detection of HE4, such as amine-modified graphene-loaded gold nanorods (Au NRs/NH_2-GS) [121], $NiFe_2O_4$NTs [122], and reduced graphene oxide-modified TiO_2 mesocrystalline hybrid material (TiO_2MCs@RGO) [123]. In particular, the ECL and PEC demonstrated ultra-high sensitivity and specificity for detecting HE4. For example, Zhang et al. developed an ECL method based on a multi-stimulus-responsive MoS_2 nanosheet (MoS_2NSs) platform to detect HE4 with high sensitivity [124]. The ECL platform consisted of three parts, namely MoS_2NSs, an AuNPs modified $NiFe_2O_4$NTs electrode modified with single-stranded DNA (DNA3), and DNA-labeled antibody (DNA1-Ab1 and DNA2-Ab2). MoS_2NSs had many excellent characteristics, such as high electrocatalytic activity, and peroxidase-like activity [125]. In addition, MoS_2NSs specifically bond to single-stranded DNA through van der Waals forces, but had a low affinity for double-stranded DNA. Especially, MoS_2NSs triggered H_2O_2 to oxidize colorless 2,20-azinobis (3-ethylbenzothiazoline)-6-sulfonic acid (ABTS) to green

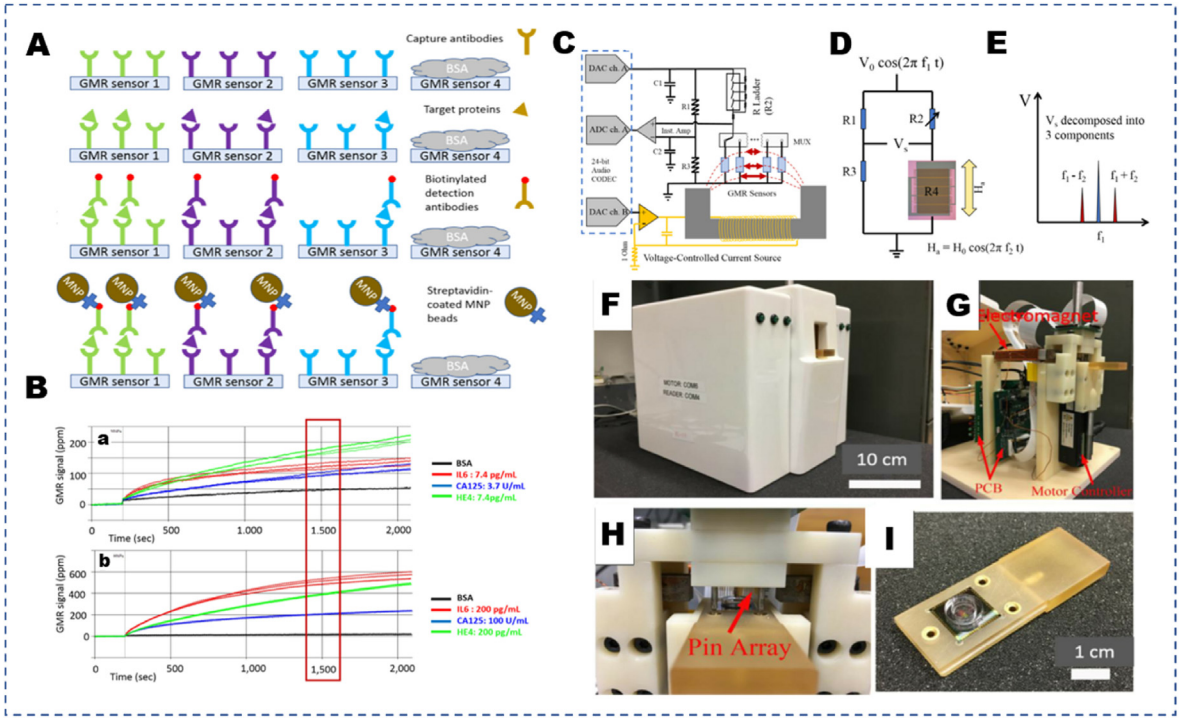

Fig. 8. GMR multiplex detection sensor system. (A)Detection mechanism and assay sequence. (Green-CA125, purple-HE4, blue-IL6 and gray-BSA.) (B) Real-time multiplex tests on GMR sensors. (C) Schematic representation of Wheatstone Bridge circuit on the multiplexing board. (D) Simplified schematic of Wheatstone Bridge. (E) Signal decomposed into a center tone and two mixed frequency components (side tones). (F) Benchtop GMR base station, with an overall size of 20 cm × 20 cm × 20 cm. (G) Design inside the base station. (H) Pin array aligning and moving close with the electrode pads of the GMR chip. (I) Reaction-well attached GMR chip on the chip holder. Reprinted with permission from Ref. [115]. Copyright 2018 Elsevier B.V.

oxidation-type ABTS ($ABTS^{\cdot+}$), by which MoS_2NSs mediated a variety of physicochemical processes, such as ECL, color change, and the generation of photothermal active $ABTS^{\cdot+}$. In the presence of HE4, HE4 triggered the linked complex to hybridize with DNA3 and greatly reduced the multiple signaling mediated MoS_2NSs. The MoS_2NSs effectively avoided false negative results through mutual calibration of multiple signals, and exhibited excellent selectivity, reproducibility, and high sensitivity for HE4 in the blood sample.

Highly porous metal-organic framework (MOF) can further increase the sensitivity of electrochemical HE4 detection. Very recently, Chen et al. developed a porphyrin-based metal-organic framework nanosphere (nPCN-224) PEC immunosensor for HE4 detection in the blood samples [126]. The PEC sensor was composed of MWCNTs/polydopamine (PDA)/AuNPs electrode and nPCN-224 all functionalized with HE4 nanobodies (Nbs) [127] (antibody with high affinity for HE4 from camel serum). After the addition of HE4, a sandwich structure complex of nPCN-224@Nbs-HE4-Nbs@MWCNTs/PDA/AuNPs was formed to generate a photoreduction current under light (Fig. 9A). Due to highly ordered porosity and high photoelectric performance of nPCN-224, the PEC sensor had a very high selectivity and sensitivity with a detection limit of 0.560 pg mL^{-1}, which is lower than most methods previously reported (Fig. 9B and C).

9. Summary and prospects

Recently, the great progresses of the early OC diagnosis are mainly driven by the discovery of new OC biomarkers, advances of separation and enrichment technology, and the innovation of detection methods. Nanomaterial-based IVDs have significantly improved the accuracy, selectivity, and sensitivity of OC biomarker detection with the deepening of interdisciplinary collaborations across oncology, pathology, biology, medicine, materials science, and nanotechnology. Nano-pattern embedded microfluidic chips, multifunctional electrochemical detection platforms, and magnetic separation platforms make it possible to analyze ultra-low levels of CTCs and exosomes in OC blood. Moreover, the resulting purified CTCs/exosomes with high integrity can further ensure downstream molecular and functional analysis. The detection of other novel biomarkers such as nucleic acids, LPA and LSR can also greatly reduce false positives and exponentially increase sensitivity through the incorporation of nanomaterials into IVD. In addition, the multifunctional nanomaterials modification of IVD can also greatly improve the accuracy of OC diagnosis by the combined detection of traditional OC biomarkers such as CA-125 and HE4. Therefore, these advances suggest that nanomaterial-based IVD has great potential for clinical application in the early diagnosis of OC.

Despite these advances, there is still a big gap to improve the accuracy of early diagnosis of OC. We believe that future work in this area will focus on the following: Firstly, exploring the preparation of new nanomaterials and the effects of nanostructure and chemical/physical properties on biomarker recognition, capture, and detection performance to further improve the specificity of marker detection. Secondly, combine more precise analysis techniques and nanotechnology to better characterize CTCs, exosomes, nucleic acids, and metabolites. Thirdly, when novel OC biomarkers are discovered, develop efficient nanomaterial-based IVD platforms for these biomarkers. In fact, these new biomarkers also need to be validated for their accuracy in clinical assays. Nanomaterials with variability and unique characteristics can facilitate the development of IVD devices to keep up with the pace of new biomarker discovery and ultimately screen out more truly accurate ones. Fourthly, the lack of standardization in the preparation of nanomaterials, construction of IVD devices, processing of samples, and analysis of data may raise serious concerns about the reliability and reproducibility of early OC diagnosis in clinical trials. Therefore, more research efforts need be done to clinically validate nanomaterial-based IVD assays and establish standardization for the transition of these platforms to clinical applications. In conclusion, nanomaterial-based IVD not only improves our understanding of OC pathology, treatment, but may have a major impact in the field of oncology. Finally, the clinical transformation of more nanomaterials-based biosensors will be realized soon in the field of early OC diagnosis with the advances of tumor biology and nanotechnology [128–131]. More effective and reliable nanomaterial-based IVD, with higher sensitivity and accuracy, smaller size, and more economical price,

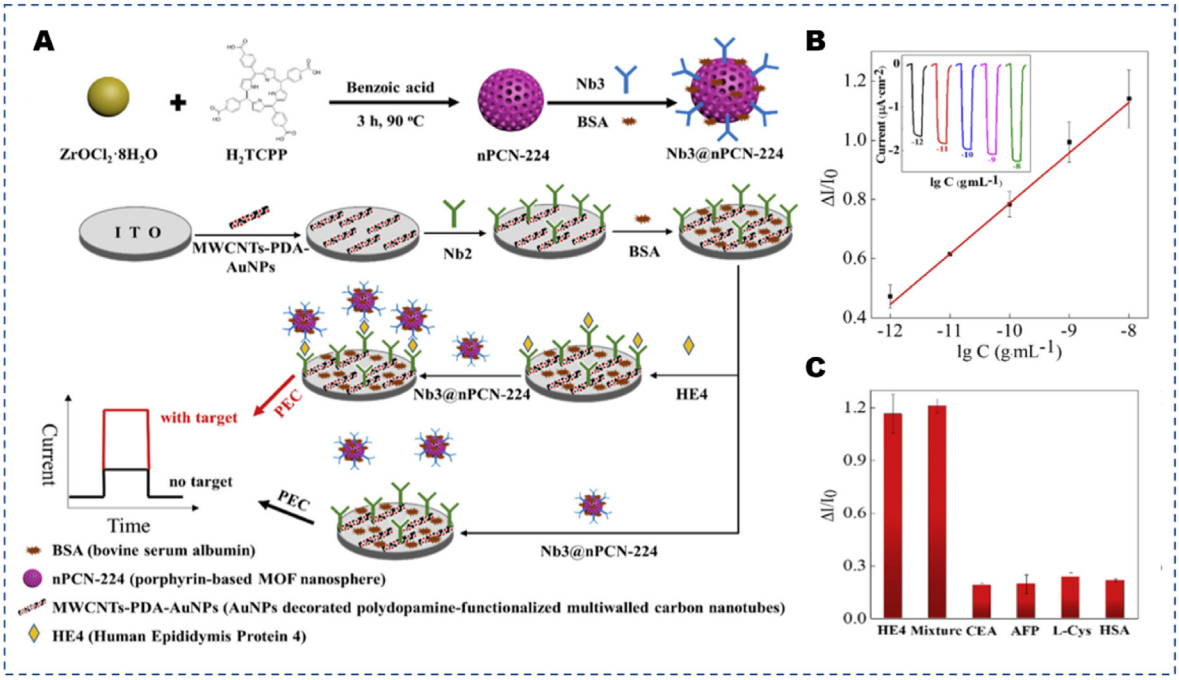

Fig. 9. (A) Scheme for the preparation of Nb3@nPCN-224 and fabrication of PEC HE4 immunosensor. (B) Calibration plot of the PEC immunoassay for the detection of different concentrations of HE4. Inset: photocurrent responses of the PEC immunosensor. (C) Photocurrent responses of the proposed immunosensor for 10.0 ng/mLHE4 compared to those for 1.00 mg/mL interferents (CEA, AFP, L-Cys, HSA) and the mixture of them in 10 mM PBS solution. Reprinted with permission from Ref. [126]. Copyright 2020 Elsevier B.V.

will be developed for clinical testing and even home self-testing.

Credit author statement

Yuqi Yang: Investigation and Curation, Writing – original draft. **Qiong Huang**: Conceptualization, Writing-Reviewing and Editing. **Zuoxiu Xiao**: Writing – original draft. **Min Liu**: Curation. **Yan Zhu**: Writing-Reviewing and Editing. **Qiaohui Chen**: Writing – original draft. **Yumei Li**: Writing-Reviewing and Editing. **Kelong Ai**: Conceptualization, Writing- Reviewing and Editing, Supervision and Administration.

Declaration of competing interest

The authors declare that they have no known competing financial interests or personal relationships that could have appeared to influence the work reported in this paper.

Acknowledgements

This work was supported by the National Natural Science Foundation, China (No. 21974134, 81974508), the Hunan Science Fund for Distinguished Young Scholar (No. 2021JJ10067), Innovation-Driven Project of Central South University (No. 202045005), Hunan Provincial Natural Science Foundation of China (No. 2021JJ31066), Changsha Science and Technology Project (No. kq2001048), Key Research Project of Ningxia Hui Autonomous Region in 2021 (Major Project) (No. 2021BEG01001).

References

[1] R.L. Siegel, K.D. Miller, H.E. Fuchs, et al., Cancer statistics, 2021[J], CA Canc. J. Clin. 71 (1) (2021) 7–33.
[2] H. Sung, J. Ferlay, R.L. Siegel, et al., Global cancer statistics 2020: GLOBOCAN estimates of incidence and mortality worldwide for 36 cancers in 185 countries [J], CA Canc. J. Clin. 71 (3) (2021) 209–249.
[3] J. Ferlay, M. Colombet, I. Soerjomataram, et al., Cancer statistics for the year 2020: an overview[J], Int. J. Cancer (2021).
[4] F. Islami, E.M. Ward, H. Sung, et al., Annual report to the nation on the status of cancer, Part 1: national cancer statistics[J], J. Natl. Canc. Inst. (2021).
[5] K.H. Kensler, C.H. Pernar, B.A. Mahal, et al., Racial and ethnic variation in PSA testing and prostate cancer incidence following the 2012 USPSTF recommendation[J], J. Natl. Canc. Inst. 113 (6) (2021) 719–726.
[6] A. Jemal, E.M. Ward, C.J. Johnson, et al., Annual report to the nation on the status of cancer, 1975-2014, featuring survival[J], J. Natl. Canc. Inst. 109 (9) (2017).
[7] B. Khiewvan, D.A. Torigian, S. Emamzadehfard, et al., An update on the role of PET/CT and PET/MRI in ovarian cancer[J], Eur. J. Nucl. Med. Mol. Imag. 44 (6) (2017) 1079–1091.
[8] X.L. Huang, Y.J. Liu, B. Yung, et al., Nanotechnology-enhanced No-wash biosensors for in vitro diagnostics of cancer[J], ACS Nano 11 (6) (2017) 5238–5292.
[9] C.H. Huang, Y.I. Park, H.Y. Lin, et al., Compact and filter-free luminescence biosensor for mobile in vitro diagnoses[J], ACS Nano 13 (10) (2019) 11698–11706.
[10] H.B. Song, Y.Y. Zhu, The in vitro diagnostics industry in China[J], View 1 (1) (2020) e5.
[11] X.M. Sun, J.J. Wan, K. Qian, Designed microdevices for in vitro diagnostics[J], Small Methods 1 (10) (2017) 1700196.
[12] S. Sharma, R. Raghav, R. O'kennedy, et al., Advances in ovarian cancer diagnosis: a journey from immunoassays to immunosensors[J], Enzym. Microb. Technol. 89 (2016) 15–30.
[13] W. Lee, S.Y. Ko, M.S. Mohamed, et al., Neutrophils facilitate ovarian cancer premetastatic niche formation in the omentum[J], J. Exp. Med. 216 (1) (2019) 176–194.
[14] S. Zhang, I. Dolgalev, T. Zhang, et al., Both fallopian tube and ovarian surface epithelium are cells-of-origin for high-grade serous ovarian carcinoma[J], Nat. Commun. 10 (2019).
[15] N. Wongkaew, M. Simsek, C. Griesche, et al., Functional nanomaterials and nanostructures enhancing electrochemical biosensors and lab-on-a-chip performances: recent progress, applications, and future perspective[J], Chem. Rev. 119 (1) (2019) 120–194.
[16] J.J.X. Wu, X.Y. Wang, Q. Wang, et al., Nanomaterials with enzyme-like characteristics (nanozymes): next-generation artificial enzymes (II)[J], Chem. Soc. Rev. 48 (4) (2019) 1004–1076.
[17] D.G. Papageorgiou, I.A. Kinloch, R.J. Young, Mechanical properties of graphene and graphene-based nanocomposites[J], Prog. Mater. Sci. 90 (2017) 75–127.
[18] T. Guo, K. Wang, G.K. Zhang, et al., A novel alpha-Fe2O3@g-C3N4 catalyst: synthesis derived from Fe-based MOF and its superior photo-Fenton performance [J], Appl. Surf. Sci. 469 (2019) 331–339.
[19] K.L. Lin, T. Yang, H.Y. Zou, et al., Graphitic C3N4 nanosheet and hemin/G-quadruplex DNAzyme-based label-free chemiluminescence aptasensing for biomarkers[J], Talanta 192 (2019) 400–406.
[20] J. Li, X. Liu, J.M. Crook, et al., 3D graphene-containing structures for tissue engineering[J], Mater. Today Chem. 14 (2019).
[21] H. Filik, A.A. Avan, Nanostructures for nonlabeled and labeled electrochemical immunosensors: simultaneous electrochemical detection of cancer markers: a review[J], Talanta (2019) 205.
[22] K.Y. Goud, S.K. Kalisa, V. Kumar, et al., Progress on nanostructured electrochemical sensors and their recognition elements for detection of mycotoxins: a review[J], Biosens. Bioelectron. 121 (2018) 205–222.
[23] M. Sharifi, M.R. Avadi, F. Attar, et al., Cancer diagnosis using nanomaterials based electrochemical nanobiosensors[J], Biosens. Bioelectron. 126 (2019) 773–784.
[24] Z. Altintas, M. Akgun, G. Kokturk, et al., A fully automated microfluidic-based electrochemical sensor for real-time bacteria detection[J], Biosens. Bioelectron. 100 (2018) 541–548.
[25] M.P. Wolf, G.B. Salieb-Beugelaar, P. Hunziker, PDMS with designer functionalities-Properties, modifications strategies, and applications[J], Prog. Polym. Sci. 83 (2018) 97–134.
[26] Y. Feng, X. Zhong, T.-T. Tang, et al., Rab27a dependent exosome releasing participated in albumin handling as a coordinated approach to lysosome in kidney disease[J], Cell Death Dis. 11 (7) (2020).
[27] D. Guo, G.Y.L. Lui, S.L. Lai, et al., RAB27A promotes melanoma cell invasion and metastasis via regulation of pro-invasive exosomes[J], Int. J. Cancer 144 (12) (2019) 3070–3085.
[28] L. Song, S. Tang, X. Han, et al., KIBRA controls exosome secretion via inhibiting the proteasomal degradation of Rab27a[J], Nat. Commun. 10 (2019).
[29] Y.T. Kang, E. Purcell, C. Palacios-Rolston, et al., Isolation and profiling of circulating tumor-associated exosomes using extracellular vesicular lipid-protein binding affinity based microfluidic device[J], Small 15 (47) (2019), e1903600.
[30] G. Van Niel, G. D'angelo, G. Raposo, Shedding light on the cell biology of extracellular vesicles[J], Nat. Rev. Mol. Cell Biol. 19 (4) (2018) 213–228.
[31] R. Kalluri, V.S. Lebleu, The biology, function, and biomedical applications of exosomes[J], Science 367 (6478) (2020) 640(. -+).
[32] M.K.S. Tang, P.Y.K. Yue, P.P. Ip, et al., Soluble E-cadherin promotes tumor angiogenesis and localizes to exosome surface[J], Nat. Commun. 9 (2018).
[33] J. Zhou, X. Li, X. Wu, et al., Exosomes released from tumor-associated macrophages transfer miRNAs that induce a treg/Th17 cell imbalance in epithelial ovarian cancer[J], Canc. Immun. Res. 6 (12) (2018) 1578–1592.
[34] H.L. Shao, H. Im, C.M. Castro, et al., New technologies for analysis of extracellular vesicles[J], Chem. Rev. 118 (4) (2018) 1917–1950.
[35] S.T.Y. Chuo, J.C.Y. Chien, C.P.K. Lai, Imaging extracellular vesicles: current and emerging methods[J], J. Biomed. Sci. 25 (2018).
[36] E.K. Sackmann, A.L. Fulton, D.J. Beebe, The present and future role of microfluidics in biomedical research[J], Nature 507 (7491) (2014) 181–189.
[37] K.D.P. Dorayappan, M.L. Gardner, C.L. Hisey, et al., A microfluidic chip enables isolation of exosomes and establishment of their protein profiles and associated signaling pathways in ovarian cancer[J], Cancer Res. 79 (13) (2019) 3503–3513.
[38] P. Zhang, X. Zhou, M. He, et al., Ultrasensitive detection of circulating exosomes with a 3D-nanopatterned microfluidic chip[J], Nat. Biomed. Eng. 3 (6) (2019) 438–451.
[39] P. Zhang, X. Zhou, Y. Zeng, Multiplexed immunophenotyping of circulating exosomes on nano-engineered ExoProfile chip towards early diagnosis of cancer [J], Chem. Sci. 10 (21) (2019) 5495–5504.
[40] F.S. Felix, L. Angnes, Electrochemical immunosensors - a powerful tool for analytical applications[J], Biosens. Bioelectron. 102 (2018) 470–478.
[41] H. Zhang, Z. Wang, F. Wang, et al., Ti3C2 MXene mediated Prussian blue in situ hybridization and electrochemical signal amplification for the detection of exosomes[J], Talanta 224 (2021) 121879.
[42] F.Z. Farhana, M. Umer, A. Saeed, et al., Isolation and detection of exosomes using Fe2O3 nanoparticles[J], ACS Appl. Nano Mater. 4 (2) (2021) 1175–1186.
[43] X.J. Liu, Q.E. Wang, J. Chen, et al., Ultrasensitive electrochemiluminescence biosensor for the detection of tumor exosomes based on peptide recognition and luminol-AuNPs@g-C3N4 nanoprobe signal amplification[J], Talanta (2021) 221.
[44] D.B. Asante, L. Calapre, M. Ziman, et al., Liquid biopsy in ovarian cancer using circulating tumor DNA and cells: ready for prime time?[J], Cancer Lett. 468 (2019) 59–71.
[45] Ovarian tumors metastasize in blood[J], Cancer Discov. 4 (9) (2014) OF2.
[46] N. Soda, B.H.A. Rehm, P. Sonar, et al., Advanced liquid biopsy technologies for circulating biomarker detection[J], J. Mater. Chem. B 7 (43) (2019) 6670–6704.
[47] X.H. Zhang, H. Li, X.Y. Yu, et al., Analysis of circulating tumor cells in ovarian cancer and their clinical value as a biomarker[J], Cell. Physiol. Biochem. 48 (5) (2018) 1983–1994.
[48] D.B. Asante, L. Calapre, M. Ziman, et al., Liquid biopsy in ovarian cancer using circulating tumor DNA and cells: ready for prime time?[J], Cancer Lett. 468 (2020) 59–71.
[49] C. Alix-Panabieres, K. Pantel, Challenges in circulating tumour cell research[J], Nat. Rev. Cancer 14 (9) (2014) 623–631.
[50] P. Banko, S.Y. Lee, V. Nagygyorgy, et al., Technologies for circulating tumor cell separation from whole blood[J], J. Hematol. Oncol. 12 (1) (2019) 48.
[51] M.K. Masud, J. Na, M. Younus, et al., Superparamagnetic nanoarchitectures for disease-specific biomarker detection[J], Chem. Soc. Rev. 48 (24) (2019) 5717–5751.
[52] C.H. Chu, R.X. Liu, T. Ozkaya-Ahmadov, et al., Hybrid negative enrichment of circulating tumor cells from whole blood in a 3D-printed monolithic device[J], Lab Chip 19 (20) (2019) 3427–3437.

[53] Z.E. Wu, Y. Pan, Z.L. Wang, et al., A PLGA nanofiber microfluidic device for highly efficient isolation and release of different phenotypic circulating tumor cells based on dual aptamers[J], J. Mater. Chem. B 9 (9) (2021) 2212–2220.
[54] H. Park, M.P. Hwang, K.H. Lee, Immunomagnetic nanoparticle-based assays for detection of biomarkers[J], Int. J. Nanomed. 8 (2013) 4543–4552.
[55] L. Wang, P. Balasubramanian, A.P. Chen, et al., Promise and limits of the CellSearch platform for evaluating pharmacodynamics in circulating tumor cells [J], Semin. Oncol. 43 (4) (2016) 464–475.
[56] K. Pantel, C. Alix-Panabieres, S. Riethdorf, Cancer micrometastases[J], Nat. Rev. Clin. Oncol. 6 (6) (2009) 339–351.
[57] V. Das, S. Bhattacharya, C. Chikkaputtaiah, et al., The basics of epithelial-mesenchymal transition (EMT): a study from a structure, dynamics, and functional perspective[J], J. Cell. Physiol. (2019).
[58] M. Yu, A. Bardia, B.S. Wittner, et al., Circulating breast tumor cells exhibit dynamic changes in epithelial and mesenchymal composition[J], Science 339 (6119) (2013) 580–584.
[59] L.P. Martin, J.A. Konner, K.N. Moore, et al., Characterization of folate receptor alpha (FRalpha) expression in archival tumor and biopsy samples from relapsed epithelial ovarian cancer patients: A phase I expansion study of the FRalpha-targeting antibody-drug conjugate mirvetuximab soravtansine[J], Gynecol. Oncol. 147 (2) (2017) 402–407.
[60] M. Scaranti, E. Cojocaru, S. Banerjee, et al., Exploiting the folate receptor alpha in oncology[J], Nat. Rev. Clin. Oncol. 17 (6) (2020) 349–359.
[61] L. Nie, F. Li, X. Huang, et al., Folic acid targeting for efficient isolation and detection of ovarian cancer CTCs from human whole blood based on two-step binding strategy[J], ACS Appl. Mater. Interfaces 10 (16) (2018) 14055–14062.
[62] F.L. Li, G.T. Yang, Z.P. Aguilar, et al., Affordable and simple method for separating and detecting ovarian cancer circulating tumor cells using BSA coated magnetic nanoprobes modified with folic acid[J], Sensor. Actuator. B Chem. 262 (2018) 611–618.
[63] N. Li, Y. Cheng, L. Chen, et al., Circulating tumour cell detection in epithelial ovarian cancer using dual-component antibodies targeting EpCAM and FR alpha [J], Ann. Oncol. 30 (2019), 581-581.
[64] X.Y. Meng, P.F. Sun, H.Y. Xu, et al., Folic acid-functionalized magnetic nanoprobes via a PAMAM dendrimer/SA-biotin mediated cascade-amplifying system for the efficient enrichment of circulating tumor cells[J], Biomater. Sci. 8 (22) (2020) 6395–6403.
[65] J.H. Ha, R. Radhakrishnan, M. Jayaraman, et al., LPA induces metabolic reprogrammingin ovarian cancer via a pseudohypoxic response[J], Cancer Res. 78 (8) (2018) 1923–1934.
[66] T. Yagi, M. Shoaib, C.E. Kuschner, et al., Challenges and inconsistencies in using lysophosphatidic acid as a biomarker for ovarian cancer[J], Cancers 11 (4) (2019).
[67] J. Li, C.D. Ji, B.Z. Lu, et al., Dually crosslinked supramolecular hydrogel for cancer biomarker sensing[J], ACS Appl. Mater. Interfaces 12 (33) (2020) 36873–36881.
[68] Y. Wang, H.W. Pei, Y. Jia, et al., Synergistic tailoring of electrostatic and hydrophobic interactions for rapid and specific recognition of lysophosphatidic acid, an early-stage ovarian cancer biomarker[J], J. Am. Chem. Soc. 139 (33) (2017) 11616–11621.
[69] K. Hiramatsu, S. Serada, T. Enomoto, et al., LSR antibody therapy inhibits ovarian epithelial tumor growth by inhibiting lipid uptake[J], Cancer Res. 78 (2) (2018) 516–527.
[70] S. Matsuzaki, K. Hiramatsu, S. Serada, et al., Lipolysis-stimulated lipoprotein receptor (LSR) can be a novel therapeutic target of ovarian cancer[J], Cancer Res. (2016) 76.
[71] D. Fang, J. Li, D. Huang, et al., Dual-modality probe based on black phosphorous and NiFe2O4 NTs for electrochemiluminescence and photothermal detection of ovarian cancer marker[J], Talanta 211 (2020) 120660.
[72] Y. Chen, S. Zhang, H. Dai, et al., A multiple mixed TiO2 mesocrystal junction based PEC-colorimetric immunoassay for specific recognition of lipolysis stimulated lipoprotein receptor[J], Biosens. Bioelectron. 148 (2020) 111809.
[73] F. Cao, J. Xiong, F. Wu, et al., Enhanced photoelectrochemical performance from rationally designed anatase/rutile TiO2 heterostructures[J], ACS Appl. Mater. Interfaces 8 (19) (2016) 12239–12245.
[74] H. Schwarzenbach, N. Nishida, G.A. Calin, et al., Clinical relevance of circulating cell-free microRNAs in cancer[J], Nat. Rev. Clin. Oncol. 11 (3) (2014) 145–156.
[75] J. Yang, S. Cheng, N. Zhang, et al., Liquid biopsy for ovarian cancer using circulating tumor cells: recent advances on the path to precision medicine[J], Biochim. Biophys. Acta Rev. Canc (1) (2022) 1877.
[76] J. Phallen, M. Sausen, V. Adleff, et al., Direct detection of early-stage cancers using circulating tumor DNA[J], Sci. Transl. Med. 9 (403) (2017).
[77] S. Lheureux, M. Braunstein, A.M. Oza, Epithelial ovarian cancer: evolution of management in the era of precision medicine[J], CA Canc. J. Clin. 69 (4) (2019) 280–304.
[78] J.C.M. Wan, C. Massie, J. Garcia-Corbacho, et al., Liquid biopsies come of age: towards implementation of circulating tumour DNA[J], Nat. Rev. Cancer 17 (4) (2017) 223–238.
[79] Cancer Genome Atlas Research N. Integrated genomic analyses of ovarian carcinoma[J], Nature 474 (7353) (2011) 609–615.
[80] C. Alix-Panabieres, H. Schwarzenbach, K. Pantel, Circulating tumor cells and circulating tumor DNA[J], Annu. Rev. Med. 63 (2012) 199–215.
[81] F. Mouliere, D. Chandrananda, A.M. Piskorz, et al., Enhanced detection of circulating tumor DNA by fragment size analysis[J], Sci. Transl. Med. 10 (466) (2018).
[82] S. Cristiano, A. Leal, J. Phallen, et al., Genome-wide cell-free DNA fragmentation in patients with cancer[J], Nature 570 (7761) (2019) 385–389.
[83] S. Mueller, N. Bley, M. Glass, et al., IGF2BP1 enhances an aggressive tumor cell phenotype by impairing miRNA-directed downregulation of oncogenic factors[J], Nucleic Acids Res. 46 (12) (2018) 6285–6303.
[84] A. Yokoi, J. Matsuzaki, Y. Yamamoto, et al., Integrated extracellular microRNA profiling for ovarian cancer screening[J], Nat. Commun. 9 (2018).
[85] A. Yokoi, J. Matsuzaki, Y. Yamamoto, et al., Integrated extracellular microRNA profiling for ovarian cancer screening[J], Nat. Commun. 9 (1) (2018) 4319.
[86] A.-M. Patch, E.L. Christie, D. Etemadmoghadam, et al., Whole-genome characterization of chemoresistant ovarian cancer[J], Nature 521 (7553) (2015) 489–494.
[87] M. Alharbi, S. Sharma, D. Guanzon, et al., miRNa signature in small extracellular vesicles and their association with platinum resistance and cancer recurrence in ovarian cancer[J], Nanomed. Nanotechnol. Biol. Med. 28 (2020) 102207.
[88] N.B. Aziz, R.G.G. Mahmudunnabi, M. Umer, et al., MicroRNAs in ovarian cancer and recent advances in the development of microRNA-based biosensors[J], Analyst 145 (6) (2020) 2038–2057.
[89] F. Mosele, J. Remon, J. Mateo, et al., Recommendations for the use of next-generation sequencing (NGS) for patients with metastatic cancers: a report from the ESMO Precision Medicine Working Group[J], Ann. Oncol. 31 (11) (2020) 1491–1505.
[90] L. He, W. Zhu, Q. Chen, et al., Ovarian cancer cell-secreted exosomal miR-205 promotes metastasis by inducing angiogenesis[J], Theranostics 9 (26) (2019) 8206–8220.
[91] C. Hu, L. Zhang, Z. Yang, et al., Graphene oxide-based qRT-PCR assay enables the sensitive and specific detection of miRNAs for the screening of ovarian cancer[J], Anal. Chim. Acta 1174 (2021) 338715.
[92] Y. Guan, O. Mayba, T. Sandmann, et al., High-throughput and sensitive quantification of circulating tumor DNA by microfluidic-based multiplex PCR and next-generation sequencing[J], J. Mol. Diagn. 19 (6) (2017) 921–932.
[93] H. Mollasalehi, E. Shajari, A colorimetric nano-biosensor for simultaneous detection of prevalent cancers using unamplified cell-free ribonucleic acid biomarkers[J], Bioorg. Chem. 107 (2021) 104605.
[94] H. Chen, Y. Xiang, R. Cai, et al., An ultrasensitive biosensor for dual-specific DNA based on deposition of polyaniline on a self-assembled multi-functional DNA hexahedral-nanostructure[J], Biosens. Bioelectron. 179 (2021) 113066.
[95] M. Xiao, W. Lai, T. Man, et al., Rationally engineered nucleic acid architectures for biosensing applications[J], Chem. Rev. 119 (22) (2019) 11631–11717.
[96] A. Malpica, K.K. Wong, The molecular pathology of ovarian serous borderline tumors[J], Ann. Oncol. 27 (1) (2016) i16–i19.
[97] N. Soda, M. Umer, N. Kashaninejad, et al., PCR-free detection of long non-coding HOTAIR RNA in ovarian cancer cell lines and plasma samples, [J]. Cancers 12 (8) (2020) 2333.
[98] H.Y. Su, X.X. Li, L. Huang, et al., Plasmonic alloys reveal a distinct metabolic phenotype of early gastric cancer[J], Adv. Mater. 33 (17) (2021) 2007978.
[99] W.K. Shu, Y. Wang, C. Liu, et al., Construction of a plasmonic chip for metabolic analysis in cervical cancer screening and evaluation[J], Small Methods 4 (4) (2020) 1900469.
[100] L. Huang, L. Wang, X.M. Hu, et al., Machine learning of serum metabolic patterns encodes early-stage lung adenocarcinoma[J], Nat. Commun. 11 (1) (2020) 3556.
[101] C.C. Pei, C. Liu, Y. Wang, et al., FeOOH@Metal-Organic framework core-satellite nanocomposites for the serum metabolic fingerprinting of gynecological cancers [J], Angew. Chem. Int. Ed. 59 (27) (2020) 10831–10835.
[102] Y. Lei, R. Zang, Z. Lu, et al., ERO1L promotes IL6/sIL6R signaling and regulates MUC16 expression to promote CA125 secretion and the metastasis of lung cancer cells[J], Cell Death Dis. 11 (10) (2020) 853.
[103] J.F. Liu, K.N. Moore, M.J. Birrer, et al., Phase I study of safety and pharmacokinetics of the anti-MUC16 antibody-drug conjugate DMUC5754A in patients with platinum-resistant ovarian cancer or unresectable pancreatic cancer [J], Ann. Oncol. 27 (11) (2016) 2124–2130.
[104] A.K. Karam, B.Y. Karlan, Ovarian cancer: the duplicity of CA125 measurement[J], Nat. Rev. Clin. Oncol. 7 (6) (2010) 335–339.
[105] M. Zhang, S. Cheng, Y. Jin, et al., Roles of CA125 in diagnosis, prediction, and oncogenesis of ovarian cancer[J], Biochim. Biophys. Acta Rev. Canc (2) (2021) 1875.
[106] K.B. Paul, V. Singh, S.R.K. Vanjari, et al., One step biofunctionalized electrospun multiwalled carbon nanotubes embedded zinc oxide nanowire interface for highly sensitive detection of carcinoma antigen-125[J], Biosens. Bioelectron. 88 (2017) 144–152.
[107] D.H. Kim, B. Dudem, J.S. Yu, High-performance flexible piezoelectric-assisted triboelectric hybrid nanogenerator via polydimethylsiloxane-encapsulated nanoflower-like ZnO composite films for scavenging energy from daily human activities[J], ACS Sustain. Chem. Eng. 6 (7) (2018) 8525–8535.
[108] K.K. Gangu, S. Maddila, S.B. Jonnalagadda, A review on novel composites of MWCNTs mediated semiconducting materials as photocatalysts in water treatment [J], Sci. Total Environ. 646 (2019) 1398–1412.
[109] V. Gedi, C.K. Song, G.B. Kim, et al., Sensitive on-chip detection of cancer antigen 125 using a DNA aptamer/carbon nanotube network platform (vol 257, pg 89, 2017)[J], Sensor. Actuator. B Chem. 257 (2018), 1150-1150.
[110] P. Schmit, E. Zinn, A. Fieldsend, et al., Multiplexed neutralizing antibody assay identifies potential epitopes on the AAV capsid[J], Mol. Ther. 28 (4) (2020), 520-520.
[111] J. Shen, W. Zhao, Z. Ju, et al., PARPi triggers the STING-dependent immune response and enhances the therapeutic efficacy of immune checkpoint blockade independent of BRCAness[J], Cancer Res. 79 (2) (2019) 311–319.
[112] M.P. Crossley, M. Bocek, K.A. Cimprich, R-loops as cellular regulators and genomic threats[J], Mol. Cell 73 (3) (2019) 398–411.

[113] S. Hamd-Ghadareh, A. Salimi, F. Fathi, et al., An amplified comparative fluorescence resonance energy transfer immunosensing of CA125 tumor marker and ovarian cancer cells using green and economic carbon dots for bio-applications in labeling, imaging and sensing[J], Biosens. Bioelectron. 96 (2017) 308–316.
[114] G. Funston, W. Hamilton, G. Abel, et al., The diagnostic performance of CA125 for the detection of ovarian and non-ovarian cancer in primary care: a population-based cohort study[J], PLoS Med. 17 (10) (2020).
[115] T. Klein, W. Wang, L.N. Yu, et al., Development of a multiplexed giant magnetoresistive biosensor array prototype to quantify ovarian cancer biomarkers [J], Biosens. Bioelectron. 126 (2019) 301–307.
[116] R.M. Williams, C. Lee, T.V. Galassi, et al., Noninvasive ovarian cancer biomarker detection via an optical nanosensor implant[J], Sci. Adv. 4 (4) (2018), eaaq1090.
[117] G. Scaletta, F. Plotti, D. Luvero, et al., The role of novel biomarker HE4 in the diagnosis, prognosis and follow-up of ovarian cancer: a systematic review[J], Expert Rev. Anticancer Ther. 17 (9) (2017) 827–839.
[118] R.G. Moore, M.C. Miller, E.E. Eklund, et al., Serum levels of the ovarian cancer biomarker HE4 are decreased in pregnancy and increase with age[J], Am. J. Obstet. Gynecol. 206 (4) (2012).
[119] K. Huhtinen, P. Suvitie, J. Hiissa, et al., Serum HE4 concentration differentiates malignant ovarian tumours from ovarian endometriotic cysts[J], Br. J. Cancer 100 (8) (2009) 1315–1319.
[120] V.P. De Carvalho, M.L. Grassi, C.D. Palma, et al., The contribution and perspectives of proteomics to uncover ovarian cancer tumor markers[J], Transl. Res. 206 (2019) 71–90.
[121] Q. Yan, L.L. Cao, H. Dong, et al., Sensitive amperometric immunosensor with improved electrocatalytic Au@Pd urchin-shaped nanostructures for human epididymis specific protein 4 antigen detection[J], Anal. Chim. Acta 1069 (2019) 117–125.
[122] J.N. Wang, J.R. Song, H.L. Zheng, et al., Application of NiFe2O4 nanotubes as catalytically promoted sensing platform for ratiometric electrochemiluminescence analysis of ovarian cancer marker[J], Sensor. Actuator. B Chem. 288 (2019) 80–87.
[123] D.D. Fang, M.A. Pan, H. Yi, et al., Enhanced electrochemiluminescence of luminol-DBAE system based on self-assembled mesocrystalline hybrid for the detection of ovarian cancer marker[J], Sensor. Actuator. B Chem. 286 (2019) 608–615.
[124] S.P. Zhang, Y.J. Chen, Y.T. Huang, et al., Design and application of proximity hybridization-based multiple stimuli-responsive immunosensing platform for ovarian cancer biomarker detection[J], Biosens. Bioelectron. (2020) 159.
[125] J.L. Wang, L.H. Sui, J. Huang, et al., MoS2-based nanocomposites for cancer diagnosis and therapy[J], Bioact. Mater. 6 (11) (2021) 4209–4242.
[126] K.Y. Chen, J.Y. Xue, Q. Zhou, et al., Coupling metal-organic framework nanosphere and nanobody for boosted photoelectrochemical immunoassay of Human Epididymis Protein 4[J], Anal. Chim. Acta 1107 (2020) 145–154.
[127] M.R. Khirehgesh, J. Sharifi, F. Safari, et al., Immunotoxins and nanobody-based immunotoxins: review and update[J], J. Drug Target. 29 (8) (2021) 848–862.
[128] G. Adeboyeje, P. Shah, S. Corman, et al., Use of BRCA testing among patients diagnosed with pancreatic cancer: analysis of commercial claims database in the United States[J], J. Clin. Oncol. 38 (29) (2020).
[129] A.S. Bercow, L. Chen, S. Chatterjee, et al., Cost of care for the initial management of ovarian cancer[J], Obstet. Gynecol. 130 (6) (2017) 1269–1275.
[130] S. Corman, H. Kale, P. Shah, et al., Trends in BRCA testing among patients diagnosed with breast cancer -a retrospective analysis of a United States commercial claims database from the PRIOR-1 study[J], Cancer Res. 81 (4) (2021).
[131] C.S. Ng, Z. Zhang, S.I. Lee, et al., CT perfusion as an early biomarker of treatment efficacy in advanced ovarian cancer: an ACRIN and GOG study[J], Clin. Cancer Res. 23 (14) (2017) 3684–3691.
[132] M. Lee, E.J. Kim, Y. Cho, et al., Predictive value of circulating tumor cells (CTCs) captured by microfluidic device in patients with epithelial ovarian cancer[J], Gynecol. Oncol. 145 (2) (2017) 361–365.
[133] S.R. Torati, K.C.S.B. Kasturi, B. Lim, et al., Hierarchical gold nanostructures modified electrode for electrochemical detection of cancer antigen CA125[J], Sensor. Actuator. B Chem. 243 (2017) 64–71.
[134] M. Hasanzadeh, R. Sahmani, E. Solhi, et al., Ultrasensitive immunoassay of carcinoma antigen 125 in untreated human plasma samples using gold nanoparticles with flower like morphology: a new platform in early stage diagnosis of ovarian cancer and efficient management[J], Int. J. Biol. Macromol. 119 (2018) 913–925.
[135] L. Farzin, S. Sadjadi, M. Shamsipur, et al., Employing AgNPs doped amidoxime-modified polyacrylonitrile (PAN-oxime) nanofibers for target induced strand displacement-based electrochemical aptasensing of CA125 in ovarian cancer patients[J], Mater. Sci. Eng. Mater. Biol. Appl. 97 (2019) 679–687.
[136] P.S. Pakchin, H. Ghanbari, R. Saber, et al., Electrochemical immunosensor based on chitosan-gold nanoparticle/carbon nanotube as a platform and lactate oxidase as a label for detection of CA125 oncomarker[J], Biosens. Bioelectron. 122 (2018) 68–74.
[137] M. Jafari, M. Hasanzadeh, E. Solhi, et al., Ultrasensitive bioassay of epitope of Mucin-16 protein (CA 125) in human plasma samples using a novel immunoassay based on silver conductive nano-ink: a new platform in early stage diagnosis of ovarian cancer and efficient management[J], Int. J. Biol. Macromol. 126 (2019) 1255–1265.
[138] X.J. Zhang, Y.Y. Wang, H.P. Deng, et al., An aptamer biosensor for CA125 quantification in human serum based on upconversion luminescence resonance energy transfer[J], Microchem. J. (2021) 161.
[139] F. Chen, Y. Liu, C.Y. Chen, et al., Respective and simultaneous detection tumor markers CA125 and STIP1 using aptamer-based fluorescent and RLS sensors[J], Sensor. Actuator. B Chem. 245 (2017) 470–476.
[140] G. Bharathi, F.R. Lin, L.W. Liu, et al., An all-graphene quantum dot Forster resonance energy transfer (FRET) probe for ratiometric detection of HE4 ovarian cancer biomarker[J], Colloids Surf. B Biointerfaces (2021) 198.
[141] M. Cadkova, A. Kovarova, V. Dvorakova, et al., Electrochemical quantum dots-based magneto-immunoassay for detection of HE4 protein on metal film-modified screen-printed carbon electrodes[J], Talanta 182 (2018) 111–115.
[142] M. Mattarozzi, M. Giannetto, M. Careri, Electrochemical immunomagnetic assay as biosensing strategy for determination of ovarian cancer antigen HE4 in human serum, J]. Talanta (2020) 217.
[143] D.D. Fang, S.P. Zhang, H. Dai, et al., An ultrasensitive ratiometric electrochemiluminescence immunosensor combining photothermal amplification for ovarian cancer marker detection[J], Biosens. Bioelectron. (2019) 146.
[144] C.Y. Wang, X.X. Ye, Z.G. Wang, et al., Molecularly imprinted photo-electrochemical sensor for human epididymis protein 4 based on polymerized ionic liquid hydrogel and gold nanoparticle/ZnCdHgSe quantum dots composite film[J], Anal. Chem. 89 (22) (2017) 12391–12398.